Bilevel Multiview Latent Space Learning

Zhe Xue, Guorong Li, Shuhui Wang, Weigang Zhang, and Qingming Huang, *Senior Member, IEEE*

***Abstract*— Different kinds of features describe different aspects of image data, and each feature can be treated as a view when we take it as a particular understanding of images. Leveraging multiple views provides a richer and comprehensive description than using only a single view. However, multiview data are often represented by high-dimensional heterogeneous features, so it is meaningful to find a low-dimensional consensus representation from multiple views. In this paper, we propose an unsupervised multiview dimensionality reduction method for images based on bilevel latent space learning. As different views have different physical meanings and statistical properties, they are not directly comparable. Therefore, we learn the comparable representation for each view in the first level. The shared and the private nature of multiview data are exploited to accurately preserve the information of each view. Then, we fuse different views into a low-dimensional representation by conducting joint matrix factorization in the second level. To guarantee the low-dimensional representation to be compact and discriminative, the intrinsic geometric structure of data is utilized. Besides, our method considers resisting the outliers and noise contained in multiview data, which may influence the learned representation and deteriorate its semantic consistency. We design appropriate optimization objectives to learn the latent spaces in different levels. Compared with the existing methods, our method could provide a more flexible multiview learning strategy that not only accurately captures the information of each view but also is robust to outliers and noise, which can obtain a more discriminative and compact low-dimensional representation. Experiments on two real-world image data sets demonstrate the advantages of our method over the existing multiview dimensionality reduction methods.**

***Index Terms*— Image and video classification, latent space, matrix factorization, multiview.**

I. Introduction

MANY real-world problems involve multiview data instances that are characterized by multiple representations. For example, images can be represented by different visual features describing color, shape, texture, and other visual information. A webpage has different contents, such as text, image, video, and so on. Different views generate different descriptions about the same instance and they can complement with each other. Compared with only using a single view, a more accurate and robust representation can be obtained by leveraging multiple views. However, directly using high-dimensional multiview features will lead to the degraded performance of the model due to the "curse of dimensionality." A practical solution is to find a low-dimensional consensus representation, which could effectively characterize the multiview data and generate better learning performance.

To address the low-dimensional representation learning problem in multiview learning, many methods have been presented [1]–[6]. Some [1]–[3] use graphs to model multiview data and then fuse all the obtained graphs into a unified graph or learn a unified embedding by enforcing the embedding of each view to be consistent. A general spectral embedding framework is first proposed for multiview dimensionality reduction [1]. Patches are introduced to represent the multiview data in [2], and then the low-dimensional representation is learned by patch alignment. Besides, matrix factorization techniques are adopted in [4]–[6] to learn a new representation from multiple views. Structured sparse principle component analysis (PCA) [7] is adopted in [5] to encode the information of each view into the low-dimensional representation. The common representation in [6] is obtained by jointly factorizing the data matrix of each view into a new common subspace with group sparse regularization.

Nevertheless, most of the existing methods only partially solved the key problems in multiview learning as follows. First, different views describe different aspects of the same instance, and some information is shared among all the views, while some independent information only exists in certain view. Taking account of the shared and the private nature can represent the information of each view more accurately and better exploit the complementary nature of multiview data. Second, real data may be distributed in a low-dimensional manifold and such nonlinearity should not be ignored. By preserving the manifold structure of data in the low-dimensional representation, a more compact and discriminative representation can be obtained. Third, multiview data often contain outliers and noise, which may greatly

Manuscript received January 27, 2016; revised April 7, 2016; accepted September 1, 2016. Date of publication September 9, 2016; date of current version February 13, 2018. This work was supported in part by the National Basic Research Program of China (973 Program) under Grant 2012CB316400 and Grant 2015CB351802; in part by the National Natural Science Foundation of China under Grant 61303153, Grant 61332016, Grant 61620106009, Grant 61572488, and Grant 61672497; in part by the 863 program of China under Grant 2014AA015202; and in part by the Bureau of Frontier Sciences and Education (CAS) under Grant QYZDJ-SSW-SYS013. This paper was recommended by Associate Editor Y. Keller. *(Corresponding authors: Guorong Li and Qingming Huang.)*

Z. Xue and G. Li are with the School of Computer and Control Engineering, University of Chinese Academy of Sciences (UCAS), Beijing 101408, China, and also with the Key Laboratory of Big Data Mining and Knowledge Management, UCAS, Beijing 101408, China (e-mail: xuezhe10@mails.ucas.ac.cn; liguorong@ucas.ac.cn).

S. Wang is with the Key Laboratory of Intelligent Information Processing of Chinese Academy of Sciences (CAS), Institute of Computing Technology, CAS, Beijing 100190, China (e-mail: wangshuhui@ict.ac.cn).

W. Zhang is with the School of Computer Science and Technology, Harbin Institute of Technology, Weihai 264209, China, and also with the University of Chinese Academy of Sciences, Chinese Academy of Sciences, Beijing 100049, China (e-mail: wgzhang@hit.edu.cn).

Q. Huang is with the School of Computer and Control Engineering, University of Chinese Academy of Sciences (UCAS), Beijing 101408, China with the Key Laboratory of Big Data Mining and Knowledge Management, UCAS, Beijing 101408, China; and also with the Key Laboratory of Intelligent Information Processing of Chinese Academy of Sciences (CAS), Institute of Computing Technology, CAS, Beijing 100190, China (e-mail: qmhuang@ucas.ac.cn).

Color versions of one or more of the figures in this paper are available online at http://ieeexplore.ieee.org.

Digital Object Identifier 10.1109/TCSVT.2016.2607842

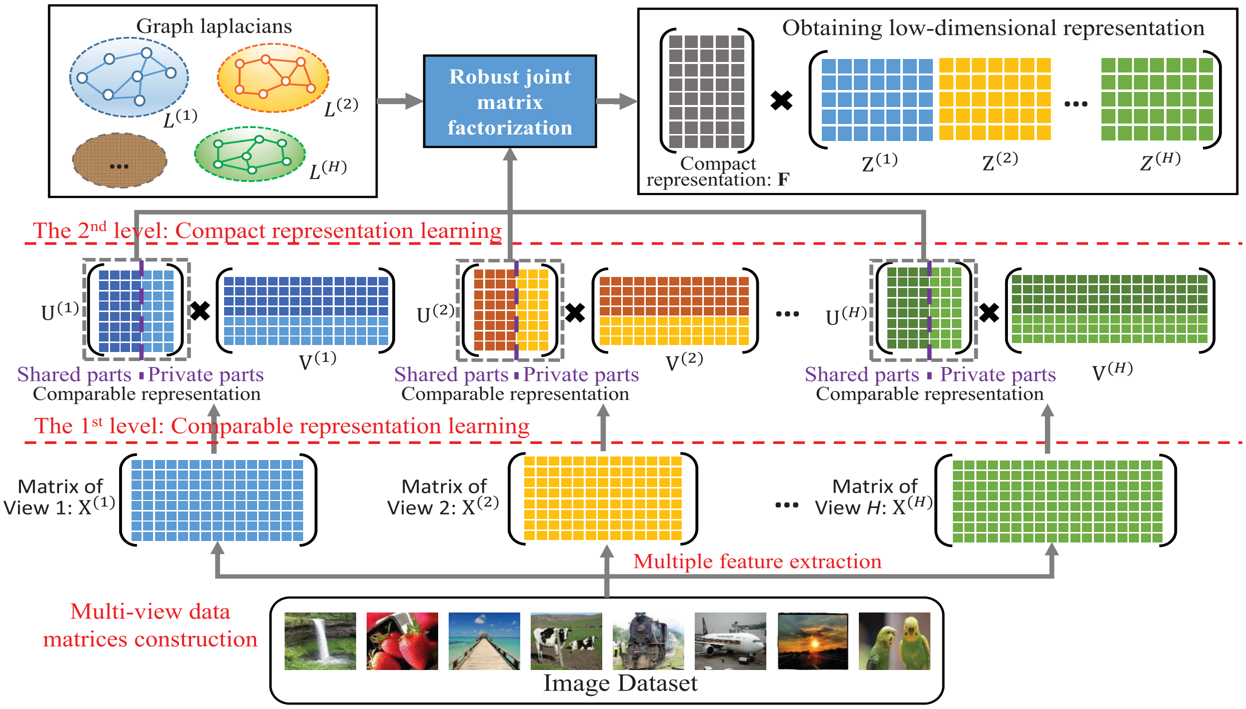
Graph laplacians
$L^{(1)}$
$L^{(2)}$
$L^{(H)}$
Robust joint matrix factorization
Obtaining low-dimensional representation
Compact representation: F
$Z^{(1)}$
$Z^{(2)}$
$Z^{(H)}$
The 2nd level: Compact representation learning
$U^{(1)}$
$V^{(1)}$
$U^{(2)}$
$V^{(2)}$
$U^{(H)}$
$V^{(H)}$
Shared parts ▪ Private parts
Comparable representation
The 1st level: Comparable representation learning
Matrix of View 1: $X^{(1)}$
Matrix of View 2: $X^{(2)}$
Matrix of View H: $X^{(H)}$
Multiple feature extraction
Multi-view data matrices construction
Image Dataset

Fig. 1. Framework of BLMV. We extract H types of visual features from data to construct the multiview matrix $\{\mathbf{X}^{(i)}\}_{i=1}^{H}$, which are represented by different colors of rectangles. In the first level, the comparable representation $\{\mathbf{U}^{(i)}\}_{i=1}^{H}$ is obtained, both shared and private parts are explored during learning. The second level learns the compact representation $\mathbf{F}$ from $\{\mathbf{U}^{(i)}\}_{i=1}^{H}$ by joint matrix factorization, and the intrinsic geometric structure $\{L^{(i)}\}_{i=1}^{H}$ of multiview data is preserved in $\mathbf{F}$.

influence the learning performance. Therefore the proposed model should be capable of accommodating these unreliable information.

In light of all the above mentioned factors, we propose an unsupervised multiview dimensionality reduction method for image data called bilevel multiview (BLMV) latent space learning, which aims to achieve better image classification and annotation performance in the learned low-dimensional subspace. Our bilevel learning strategy not only accurately captures the independent information of each view but also effectively resists the noise during the low-dimensional representation learning. In addition, the discriminating power of the learned representation can be improved by preserving the local geometric structure of multiview data. The framework of BLMV is shown in Fig. 1. Since different views with different physical meanings are not directly comparable, the objective of the first level is to learn *comparable representation* for each view (matrix $\mathbf{U}^{(i)}$ in Fig. 1). This representation is obtained by nonnegative matrix factorization (NMF) [8], which provides naturally interpretable latent spaces. Considering the shared and private information of views, the latent spaces are divided into shared and private parts. The shared parts are assumed to be consistent with each other to leverage the complementary nature of multiview data, and the private parts are learned adaptively by utilizing group sparse regularization. Consequently, the comparable representation accurately encodes the information of each view. In the second level, we conduct dimensionality reduction for the comparable representation and denote it as *compact representation* (matrix $\mathbf{F}$ in Fig. 1). By jointly factorizing the comparable representation toward a unified representation, the information of each view can be effectively fused into the learned latent space. Meanwhile, the nonlinearity structure of multiview data, which can be modeled by nearest neighbor graphs, is preserved into the learned compact representation. Taking account for the different description abilities of different views and the noise contained in multiview data, we estimate the weight for each view and introduce the $\ell_{2,1}$-norm into the loss function, which endows our model with resistancy to the unreliable views and robustness to noise and outliers.

We incorporate the learning of *comparable representation* and *compact representation* into a joint optimization framework, which learns the optimal consensus low-dimensional representation from multiple views. To solve the proposed objective function, an efficient iterative algorithm is derived and the convergence can be rigorously guaranteed. We conduct several image classification and annotation experiments on two real-world image data sets to demonstrate the effectiveness of the learned low-dimensional representation. Experimental results show the promising performance of BLMV over the existing methods. The main contributions of this paper can be summarized as follows.

1) A flexible multiview dimensionality reduction method based on bilevel learning strategy is proposed. By designing appropriate optimization objectives in different levels, the information of each view can be more effectively captured and encoded into the low-dimensional representation.
2) Both shared and private latent factors of multiple views are explored during the comparable

representation learning. Through imposing reasonable regularization on different types of latent factors, the proposed method better takes advantage of the complementary properties of multiview data.

3) The proposed method exploits the manifold structure of each view to reveal the nonlinearity inherent in data, which makes the learned low-dimensional representation more compact and discriminative. Furthermore, the robustness of the method is improved by estimating the different importance of views and adopting $\ell_{2,1}$-norm loss function for multiview fusion.

The rest of this paper is organized as follows. We introduce the related work in Section II. Then, we elaborate the proposed model, optimization scheme, and the convergence proof in Sections III and IV. Section V presents the experimental results on image classification and annotation. Finally, we conclude this paper in Section VI.

II. Related Work

Multiview learning deals with data described in multiple views and exploits the multiple descriptions to improve the learning performance. Many multiview works have been proposed for supervised learning [9]–[12] and unsupervised learning [1], [2], [13]–[15]. This paper focuses on the latter. Most of the existing multiview methods adopt two principles for learning tasks [16]. The first one is to make different views consistent by minimizing the disagreement of each view. The second principle assumes that each view contains some knowledge that the others do not contain, and thus different views can complement with each other. By adopting the two properties, multiview learning methods exploit knowledge from multiple sources and achieve better performance than single-view-based methods.

For the first principle, some works try to make the learning results of different views agree with each other. Canonical correlation analysis (CCA) extracts a common subspace from two views by maximizing the correlation among them. Chaudhuri *et al.* [17] adopt CCA to project multiview data onto a common low-dimensional subspace for clustering. By constructing a graph for each view, some methods [18]–[20] adopt spectral clustering techniques to learn a consensus representation from multiple views. Cai *et al.* [18] minimize the distance of the low-dimensional embedding of each view to obtain the unified clustering results. Considering the different importance of views, Huang *et al.* [19] assign a weight to each view, which reflects its importance. This strategy makes the learning results more accurate and robust. Patch is used in [2] and [21] to model the local structure of a sample on a view. Then, the unified representation is obtained by global coordinate alignment, which makes all the low-dimensional embedding of each view consistent with each other.

The second principle tries to exploit the complementary nature of multiview data. Cotraining method [22] is originally proposed in semisupervised learning, and then it is used for multiview learning. It assumes that the samples labeled by predictors on one view are useful for training predictors on other views. The two predictors can exchange the complementary information during cotraining process [3], [23]. By constructing a kernel for each view, multiple kernel learning (MKL) aims to combine multiple kernels together to obtain an optimal kernel. This kernel contains complementary information of different views and provides a more comprehensive measurement of similarity. Lin *et al.* [24] generalize the framework of MKL for dimensionality reduction, which provides convenience of using multiple image features.

Furthermore, some multiview works [4], [5], [25], [26] consider the shared and independent parts of each view to more accurately preserve the multiview information. Structured sparsity is used in [4] to separate the latent space into shared and independent parts for human pose estimation. The independent information of each view is first encoded into a matrix, and then structured sparse PCA [7] is used to learn the low-dimensional representation in [5]. A semisupervised latent factor learning method is proposed in [25], where the shared parts are made consistent with each other to exploit the complementary information.

Many works have shown that image data are more likely to reside on a low-dimensional submanifold of the ambient space [27]–[29]. The traditional dimensionality reduction methods, such as PCA and NMF, ignore the possible nonlinearity inherent in data, while such nonlinearity can be preserved by manifold learning methods. So some studies, such as embedding learning [28], [30], [31], feature extraction [29], [32]–[34], and clustering [35]–[37], are developed based on manifold learning. These works adopt the locally invariant property, i.e., if two samples are close in the intrinsic geometry of data manifold, then, they should have similar embeddings. Both single view [38], [39] and multiview methods [40] demonstrate that exploiting the intrinsic manifold structure of data can enhance the discriminating power of the learned latent space and further improve the learning performance. It should be noted that [38] may suffer from trivial solutions when directly adding the manifold regularization to the objective function [41]. Another constraint should be imposed to make the problem well-defined and obtain more reliable solutions [41]–[44].

The real data may contain undesirable noises and outliers and the commonly adopted least square error function is vulnerable to the unreliable data. To improve the robustness of the model, $\ell_{2,1}$-norm is introduced in [45]–[47] to cope with the noise and outliers. Compared with adopting least square function, the errors generated by outliers cannot dominate the objective function, because they are not squared with $\ell_{2,1}$-norm, so that more robust solutions can be obtained. To solve $\ell_{2,1}$-norm minimization problem, Nie *et al.* [45], [48] first develop an efficient algorithm whose convergence can be guaranteed and then extent it to solve other general $\ell_{2,1}$-norm minimization problems.

III. Bilevel Multiview Latent Space Learning

A. Preliminary

For an arbitrary matrix $\mathbf{A}$, the (i, j)th entry, the ith row, and the jth column are denoted by $\mathbf{A}_{ij}$, $\mathbf{A}_{i\cdot}$, and $\mathbf{A}_{\cdot j}$, respectively.

$Tr[\mathbf{A}]$ is the trace of $\mathbf{A}$. $\mathbf{A}\odot\mathbf{B}$ and $\mathbf{A}\oslash\mathbf{B}$ represent elementwise multiplication and division of matrices $\mathbf{A}$ and $\mathbf{B}$, respectively. $(\mathbf{A}, \mathbf{B})$ represents the horizontal concatenation of $\mathbf{A}$ and $\mathbf{B}$, and $(\mathbf{A}; \mathbf{B})$ is the vertical concatenation of them. $\mathbf{1}_M \in \mathbb{R}^{M\times 1}$ denotes a vector of ones. For $\mathbf{A} \in \mathbb{R}^{N\times M}$, the Frobenius norm is $||\mathbf{A}||_F$, and $\ell_{2,1}$-norm is defined as

$$\|\mathbf{A}\|_{2,1} = \sum_{i=1}^{N}\sqrt{\sum_{j=1}^{M}\mathbf{A}_{ij}^2}. \quad (1)$$

NMF imposes nonnegative constraints on the learned latent space and provides a more interpretable and meaningful representation. Given a nonnegative matrix $\mathbf{X} = [x_1, x_2, \ldots, x_n]^T \in \mathbb{R}^{N\times M}$, each row of $\mathbf{X}$ represents a sample. NMF aims to factorize $\mathbf{X}$ into two nonnegative matrices

$$\mathbf{X} \approx \mathbf{U}\mathbf{V} \quad (2)$$

where $\mathbf{U} \in \mathbb{R}^{N\times K}$ and $\mathbf{V} \in \mathbb{R}^{K\times M}$. We usually have $K \ll N$ and $K \ll M$ in practice. $\mathbf{V}$ can be regarded as the learned basis representing the original data $\mathbf{X}$. Each row of $\mathbf{U}$ is the low-dimensional representation of each sample with respect to basis $\mathbf{V}$.

Given multiview data set consisting of N image samples with H views, they can be denoted by a set of matrices $\mathcal{X} = \{\mathbf{X}^{(i)} \in \mathbb{R}^{N\times M_i}\}_{i=1}^{H}$, where M_i is the dimensionality of the ith view. Our objective is to learn the compact representation of images $\mathbf{F} \in \mathbb{R}^{N\times R}$, where $R < M_i, \forall i = 1, \ldots, H$.

B. Comparable Representation Learning

In the first level, we want to learn the comparable representation from heterogeneous image features. Since NMF can provide naturally interpretable and meaningful latent spaces, we adopted it here to make multiple views with different properties comparable in the learned nonnegative latent spaces. The data matrix is factorized as $\mathbf{X}^{(i)} = \mathbf{U}^{(i)}\mathbf{V}^{(i)}$, where $\mathbf{U}^{(i)} \in \mathbb{R}^{N\times K}$ is the learned comparable representation for the ith view and $\mathbf{V}^{(i)} \in \mathbb{R}^{K\times M_i}$ is the learned basis matrix. Meanwhile, the comparable representation should be capable of accurately representing the information of each view, so the shared and private properties of multiview data are exploited. We assume that the latent factors of each view are composed of shared and private parts. Shared parts referred to the latent factors that are used for generating all views, while private parts are only used for generating certain view. Taking account of this, the basis matrix is constructed as $\mathbf{V}^{(i)} = (\mathbf{V}_S^{(i)}; \mathbf{V}_P^{(i)})$, where $\mathbf{V}_S^{(i)} \in \mathbb{R}^{K_S\times M_i}$ represents the shared part of latent factors and $\mathbf{V}_P^{(i)} \in \mathbb{R}^{K_P\times M_i}$ is the private part, $K = K_S + K_P$. The coefficient matrix is also constructed as $\mathbf{U}^{(i)} = (\mathbf{U}_S^{(i)}, \mathbf{U}_P^{(i)})$, where the shared and private parts are $\mathbf{U}_S^{(i)} \in \mathbb{R}^{N\times K_S}$ and $\mathbf{U}_P^{(i)} \in \mathbb{R}^{N\times K_P}$, respectively. To control the proportion of the latent factors of shared parts and private parts, we introduce parameter $\theta = K_S/K$, which reflects the importance of shared parts in comparable representation learning. Thus, we have $K_S = ROUND(\theta \cdot K)$ and $K_P = K - K_S$.

Next, how to accurately learn the shared and private parts according to the property of each view is the critical problem. For private parts learning, we adopt group sparsity regularization, which is an effective technique to discover meaningful latent factors in latent space learning [4], [6]. To learn the private latent factors of each view according to its property, we impose $\ell_{2,1}$-norm on private parts of latent factors $\mathbf{V}_P^{(i)}$, which encourages some rows to be zeroed out. The intuition behind this is that we expect the private part of each view to depend on a subset of the latent dimensions, i.e., $\widetilde{K} \le K_P$, where $\widetilde{K}$ is the number of the learned latent factors in $\mathbf{V}_P^{(i)}$. By using this regularization, the private latent factors of each view can be learned adaptively. For shared parts learning, as the shared parts of different views refer to the same latent factors and they are directly comparable, we make the coefficients of shared parts consistent to leverage complementary information of multiple views. Although several regularization functions can be used to make them consistent [3], [49], considering the complexity of the proposed model, we adopt a simple and efficient regularization manner and define the objective function as

$$\begin{aligned}&\mathcal{O}_{cp}(\mathbf{U}^{(i)}, \mathbf{V}^{(i)})\\ &\quad = \min \sum_{i=1}^{H}\big[\big\|\mathbf{X}^{(i)} - \big(\mathbf{U}_S^{(i)}, \mathbf{U}_P^{(i)}\big)\big(\mathbf{V}_S^{(i)}; \mathbf{V}_P^{(i)}\big)\big\|_F^2\\ &\qquad + \eta\big\|\mathbf{V}_P^{(i)}\big\|_{2,1}\big] + \lambda\sum_{i=1}^{H-1}\sum_{j=i+1}^{H}\big\|\mathbf{U}_S^{(i)} - \mathbf{U}_S^{(j)}\big\|_F^2\\ &\qquad \text{s.t. } \mathbf{U}^{(i)} \ge 0, \quad \mathbf{V}^{(i)} \ge 0 \quad \forall i = 1, 2, \ldots, H \end{aligned} \quad (3)$$

where η and λ are two parameters to control the strength of group sparsity and consistent regularization.

C. Compact Representation Learning

The objective of the second level is to learn the compact representation $\mathbf{F} \in \mathbb{R}^{N\times R}$ from the comparable representation $\{\mathbf{U}^{(i)}\}_{i=1}^{H}$. We expect to encode the multiview information into the compact representation, and another matrix factorization process is conducted. However, there are three issues that should be noticed. First, the description ability of different views is different. Some views generate more reliable description than the others and it is preferable to selecting these views for representation. Second, for the learned comparable representation $\{\mathbf{U}^{(i)}\}_{i=1}^{H}$, some views may contain inaccurate description of multiview data and noise, which makes the learned compact representation deviate from the true value. Third, the intrinsic manifold structure of multiview data should be preserved in compact representation to improve its discriminative power.

A direct solution is concatenating $\{\mathbf{U}^{(i)}\}_{i=1}^{H}$ into a new matrix $\mathbf{U} = (\mathbf{U}^{(1)}, \mathbf{U}^{(2)}, \ldots, \mathbf{U}^{(H)})$, which contains the information of all views. By factorizing $\mathbf{U}$, the multiview information can be encoded into the compact representation. However, this strategy treats all views equally important during fusion. The contribution of different views on the final result $\mathbf{F}$ should be different. Therefore, a more reasonable method is first let $\|\mathbf{U} - \mathbf{F}\mathbf{Z}\|_F = \sum_{i=1}^{H}\|\mathbf{U}^{(i)} - \mathbf{F}\mathbf{Z}^{(i)}\|_F$, where $\mathbf{Z} = (\mathbf{Z}^{(1)}, \mathbf{Z}^{(2)}, \ldots, \mathbf{Z}^{(H)}), \mathbf{Z}^{(i)} \in \mathbb{R}^{R\times K}$. Then, we assign a weight to each view to represent its importance.

The view that achieves smaller factorization residual is considered to be more reliable. In addition, we need a robust loss function to cope with the outliers and noise contained in each view. By encouraging the rowwise sparsity of the residual matrix, $\ell_{2,1}$-norm accommodates outliers and noise in a better way than standard one, and it has been adopted in several robust learning tasks [46], [47]. So, we introduce $\ell_{2,1}$-norm penalty to improve the robustness, and the compact representation can be learned by solving the objective

$$\begin{aligned}&\mathcal{O}_{pt}(\mathbf{U}^{(i)}, \mathbf{F}, \mathbf{Z}^{(i)}, \gamma_i)\\&\quad= \min \sum_{i=1}^{H} \gamma_i{}^P (\|\mathbf{U}^{(i)} - \mathbf{F}\mathbf{Z}^{(i)}\|_{2,1})\\&\quad\quad \text{s.t. } \mathbf{F} \geq 0, \quad \mathbf{Z}^{(i)} \geq 0, \quad \gamma_i \geq 0\\&\quad\quad\quad \forall i = 1, \ldots, H, \quad \sum_{i=1}^{H} \gamma_i = 1\end{aligned} \tag{4}$$

where γ_i is the weight assigned to the ith view indicating the importance of that view. The exponent $P \geq 1$ is a parameter to control the smoothness of weights γ. $P = 1$ can lead to completely sparse weights, in which only a single view is selected. For $P > 1$, the weights will become smoother as the increase of the value of P.

Furthermore, we expect to capture the intrinsic manifold structure of data, which can be effectively modeled by a nearest neighbor graph. Given N samples $\{x_i\}_{i=1}^N$ with H views, we construct a p-nearest neighbor graph $\mathbf{G}^{(h)}$ with affinity matrix $\mathbf{W}^{(h)} \in \mathbb{R}^{N \times N}$ for the hth view. Then, each graph encodes the local geometric structure information of the corresponding view. Gaussian kernel is one of the most commonly used similarity and we have $\mathbf{W}_{ij}^{(h)} = exp(-||x_i - x_j||^2/2\sigma^2)$. Then, the graph Laplacian is defined as $\mathbf{L}^{(h)} = \mathbf{D}^{(h)} - \mathbf{W}^{(h)}$, where $\mathbf{D}^{(h)}$ is a diagonal matrix and $\mathbf{D}_{ii}^{(h)} = \sum_l \mathbf{W}_{il}^{(h)}$. However, it is infeasible to directly encode multiple Laplacian matrices $\{\mathbf{L}^{(h)}\}_{h=1}^H$ into the compact representation $\mathbf{F}$. Considering the different importance of views and make the reliable views contribute more, we also impose weights on each graph Laplacian matrix when encoding the structure information. Thus, the objective function for learning compact representation is revised as

$$\begin{aligned}&\mathcal{O}_{pt}(\mathbf{U}^{(i)}, \mathbf{F}, \mathbf{Z}^{(i)}, \gamma_i)\\&\quad= \min \sum_{i=1}^{H} \gamma_i{}^P [\|\mathbf{U}^{(i)} - \mathbf{F}\mathbf{Z}^{(i)}\|_{2,1} + \beta Tr(\mathbf{F}^T \mathbf{L}^{(i)} \mathbf{F})]\\&\quad \text{s.t. } \mathbf{Z}^{(i)} \geq 0, \gamma_i \geq 0 \quad \forall i = 1, \ldots, H, \quad \sum_{i=1}^{H} \gamma_i = 1\\&\quad \mathbf{F} \geq 0, \quad \mathbf{F}\mathbf{1}_R = \mathbf{1}_N\end{aligned} \tag{5}$$

where β controls the strength of preserving structure information. We impose the ℓ_1 normalization constraints on the rows of $\mathbf{F}$ to handle the trivial solution problem [41], so that more reliable solutions can be obtained.

D. Unified Objective Function

To learn the optimal comparable representation and compact representation simultaneously, the ultimate objective of BLMV is formulated by integrating the two subproblems into a unified function

$$\begin{aligned}&\mathcal{O}_U(\mathbf{U}^{(i)}, \mathbf{V}^{(i)}, \mathbf{F}, \mathbf{Z}^{(i)}, \gamma_i) = \mathcal{O}_{cp} + \mathcal{O}_{pt}\\&= \min \sum_{i=1}^{H} \big[\big\|\mathbf{X}^{(i)} - \big(\mathbf{U}_S^{(i)}, \mathbf{U}_P^{(i)}\big)\big(\mathbf{V}_S^{(i)}; \mathbf{V}_P^{(i)}\big)\big\|_F^2 + \eta \big\|\mathbf{V}_P^{(i)}\big\|_{2,1}\big]\\&\quad + \lambda \sum_{i=1}^{H-1} \sum_{j=i+1}^{H} \big\|\mathbf{U}_S^{(i)} - \mathbf{U}_S^{(j)}\big\|_F^2\\&\quad + \sum_{i=1}^{H} \gamma_i{}^P \big[\big\|\mathbf{U}^{(i)} - \mathbf{F}\mathbf{Z}^{(i)}\big\|_{2,1} + \beta Tr(\mathbf{F}^T \mathbf{L}^{(i)} \mathbf{F})\big]\\&\quad \text{s.t. } \mathbf{U}^{(i)} \geq 0, \quad \mathbf{V}^{(i)} \geq 0, \quad \mathbf{Z}^{(i)} \geq 0, \gamma_i \geq 0\\&\quad\quad \forall i = 1, \ldots, H, \quad \mathbf{F} \geq 0, \quad \mathbf{F}\mathbf{1}_R = \mathbf{1}_N, \quad \sum_{i=1}^{H} \gamma_i = 1.\end{aligned} \tag{6}$$

By solving problem (6), we can obtain the compact representation $\mathbf{F}$.

IV. Optimization

Apparently, problem (6) is not convex over all variables $\mathbf{U}^{(i)}, \mathbf{V}^{(i)}, \mathbf{F}, \mathbf{Z}^{(i)}$, and γ_i simultaneously, so we derive an iteration optimization algorithm to solve it. In each iteration, only one variable is updated, while the others remain unchanged. We adopt the multiplicative iteration method to solve $\mathbf{U}^{(i)}, \mathbf{V}^{(i)}$, and $\mathbf{Z}^{(i)}$. The detailed derivation of updating rule for $\mathbf{U}^{(i)}$ is provided in Section IV-A. Since the derivation of updating rules of $\mathbf{V}^{(i)}$ and $\mathbf{Z}^{(i)}$ is similar to $\mathbf{U}^{(i)}$, we directly present the updating rules. Since $\mathbf{F}$ is imposed by an ℓ_1 normalization constraint, we introduce the method developed in [42] and [43] to solve $\mathbf{F}$ (Section IV-B). γ_i can be solved by using Lagrange multiplier method (Section IV-C). Next, the convergence proof of our algorithm is provided, and then we analyze the computational complexity of the proposed algorithm. The optimization process is summarized in Algorithm 2.

A. Update $\mathbf{U}^{(i)}, \mathbf{V}^{(i)}$, and $\mathbf{Z}^{(i)}$

We derive the updating rules for the ith view. The Lagrange multipliers ϕ_{jk} are introduced for constraint $\mathbf{U}_{jk}^{(i)} \geq 0$, and we denote them by a matrix $\Phi = [\phi_{jk}]$. Since $\mathbf{U}^{(i)}$ is made up by two parts $(\mathbf{U}_S^{(i)}, \mathbf{U}_P^{(i)})$, we also separate $\Phi = (\Phi_S, \Phi_P)$ and $\mathbf{Z}^{(i)} = (\mathbf{Z}_S^{(i)}, \mathbf{Z}_P^{(i)})$, where $\Phi_S \in \mathbb{R}^{N \times K_S}$, $\Phi_P \in \mathbb{R}^{N \times K_P}$, $\mathbf{Z}_S^{(i)} \in \mathbb{R}^{N \times K_S}$, and $\mathbf{Z}_P^{(i)} \in \mathbb{R}^{N \times K_P}$. In order to solve $\mathbf{U}^{(i)}$, we keep the parts, which are related to $\mathbf{U}^{(i)}$ from $\mathcal{O}_U$, and the Lagrange is

$$\begin{aligned}\mathcal{L}(\mathbf{U}^{(i)}) &= \big\|\mathbf{X}^{(i)} - \big(\mathbf{U}_S^{(i)}, \mathbf{U}_P^{(i)}\big)\big(\mathbf{V}_S^{(i)}; \mathbf{V}_P^{(i)}\big)\big\|_F^2\\&\quad + \lambda \sum_{j=1}^{H} \big\|\mathbf{U}_S^{(i)} - \mathbf{U}_S^{(j)}\big\|_F^2 + \gamma_i{}^P \big\|\big(\mathbf{U}_S^{(i)}, \mathbf{U}_P^{(i)}\big)\\&\quad - \mathbf{F}\big(\mathbf{Z}_S^{(i)}, \mathbf{Z}_P^{(i)}\big)\big\|_{2,1} - Tr\big[\mathbf{U}_S^{(i)} \Phi_S^T\big] - Tr\big[\mathbf{U}_P^{(i)} \Phi_P^T\big].\end{aligned} \tag{7}$$

The partial derivative of $\mathcal{L}(\mathbf{U}^{(i)})$ with respect to $\mathbf{U}_S^{(i)}$ is

$$\begin{aligned}\frac{\partial\mathcal{L}(\mathbf{U}^{(i)})}{\partial\mathbf{U}_S^{(i)}} &= -2\mathbf{X}^{(i)}\mathbf{V}_S^{(i)^T} + 2\mathbf{U}_S^{(i)}\mathbf{V}_S^{(i)}\mathbf{V}_S^{(i)^T} + 2\mathbf{U}_P^{(i)}\mathbf{V}_P^{(i)}\mathbf{V}_S^{(i)^T} \\ &\quad + 2\lambda\sum_{j=1}^{H}\left(\mathbf{U}_S^{(i)} - \mathbf{U}_S^{(j)}\right) + 2\gamma_i^P\left(\Lambda_1^{(i)}\mathbf{U}_S^{(i)} - \Lambda_1^{(i)}\mathbf{F}\mathbf{Z}_S^{(i)}\right) - \Phi_S \end{aligned} \tag{8}$$

where we use $\Lambda_1^{(i)}$ to represent a diagonal matrix with elements $(\Lambda_1^{(i)})_{ll} = (1/(2\|(\mathbf{U}_S^{(i)} - \mathbf{F}\mathbf{Z}_S^{(i)})_{l\cdot}\|))$, and the diagonal matrices in the following parts are also expressed in this way.

Using the Karush–Kuhn–Tuckre condition $(\Phi_S)_{jk}(\mathbf{U}_S^{(i)})_{jk} = 0$, we obtain the updating rule

$$\begin{aligned}&\left(\mathbf{U}_S^{(i)}\right)_{jk} \leftarrow \left(\mathbf{U}_S^{(i)}\right)_{jk}\nabla_{\mathbf{U}_S^{(i)}}, \quad \text{and } \nabla_{\mathbf{U}_S^{(i)}} \\ &= \frac{\left(\mathbf{X}^{(i)}\mathbf{V}_S^{(i)^T} + \lambda\sum_{j=1}^{H}\mathbf{U}_S^{(j)} + \gamma_i^P\Lambda_1^{(i)}\mathbf{F}\mathbf{Z}_S^{(i)}\right)_{jk}}{\left(\mathbf{U}_S^{(i)}\mathbf{V}_S^{(i)}\mathbf{V}_S^{(i)^T} + \mathbf{U}_P^{(i)}\mathbf{V}_P^{(i)}\mathbf{V}_S^{(i)^T} + \lambda H\mathbf{U}_S^{(i)} + \gamma_i^P\Lambda_1^{(i)}\mathbf{U}_S^{(i)}\right)_{jk}}.\end{aligned} \tag{9}$$

Similarly, the updating rules for $\mathbf{U}_P^{(i)}$, $\mathbf{V}^{(i)}$, and $\mathbf{Z}^{(i)}$ can be obtained as

$$\begin{aligned}&\left(\mathbf{U}_P^{(i)}\right)_{jk} \leftarrow (\mathbf{U}_P^{(i)})_{jk}\nabla_{\mathbf{U}_P^{(i)}}, \quad \text{and } \nabla_{\mathbf{U}_P^{(i)}} \\ &= \frac{\left(\mathbf{X}^{(i)}\mathbf{V}_P^{(i)^T} + \gamma_i^P\Lambda_2^{(i)}\mathbf{F}\mathbf{Z}_P^{(i)}\right)_{jk}}{\left(\mathbf{U}_S^{(i)}\mathbf{V}_S^{(i)}\mathbf{V}_P^{(i)^T} + \mathbf{U}_P^{(i)}\mathbf{V}_P^{(i)}\mathbf{V}_P^{(i)^T} + \gamma_i^P\Lambda_2^{(i)}\mathbf{U}_P^{(i)}\right)_{jk}}\end{aligned} \tag{10}$$

$$\left(\mathbf{V}_S^{(i)}\right)_{jk} \leftarrow \left(\mathbf{V}_S^{(i)}\right)_{jk}\frac{\left(\mathbf{U}_S^{(i)^T}\mathbf{X}^{(i)}\right)_{jk}}{\left(\mathbf{U}_S^{(i)^T}\mathbf{U}_S^{(i)}\mathbf{V}_S^{(i)} + \mathbf{U}_S^{(i)^T}\mathbf{U}_P^{(i)}\mathbf{V}_P^{(i)}\right)_{jk}} \tag{11}$$

$$\begin{aligned}&\left(\mathbf{V}_P^{(i)}\right)_{jk} \leftarrow \left(\mathbf{V}_P^{(i)}\right)_{jk}\nabla_{\mathbf{V}_P^{(i)}}, \quad \text{and } \nabla_{\mathbf{V}_P^{(i)}} \\ &= \frac{\left(\mathbf{U}_P^{(i)^T}\mathbf{X}^{(i)}\right)_{jk}}{\left(\mathbf{U}_P^{(i)^T}\mathbf{U}_S^{(i)}\mathbf{V}_S^{(i)} + \mathbf{U}_P^{(i)^T}\mathbf{U}_P^{(i)}\mathbf{V}_P^{(i)} + \eta\Lambda_3^{(i)}\mathbf{V}_P^{(i)}\right)_{jk}}\end{aligned} \tag{12}$$

$$\mathbf{Z}_{jk}^{(i)} \leftarrow \mathbf{Z}_{jk}^{(i)}\frac{\left(\mathbf{F}^T\Lambda_4^{(i)}\mathbf{U}^{(i)}\right)_{jk}}{\left(\mathbf{F}^T\Lambda_4^{(i)}\mathbf{F}\mathbf{Z}^{(i)}\right)_{jk}} \tag{13}$$

where $(\Lambda_2^{(i)})_{ll} = (1/(2\|(\mathbf{U}_P^{(i)} - \mathbf{F}\mathbf{Z}_P^{(i)})_{l\cdot}\|))$, $(\Lambda_3^{(i)})_{ll} = (1/(2\|(\mathbf{V}_P^{(i)})_{l\cdot}\|))$, and $(\Lambda_4^{(i)})_{ll} = (1/(2\|(\mathbf{U}^{(i)} - \mathbf{F}\mathbf{Z}^{(i)})_{l\cdot}\|))$.

B. Update F

By keeping the related parts of $\mathbf{F}$ in $\mathcal{O}_U$, we obtain the minimization problem

$$\begin{aligned}&\min S(\mathbf{F}) \\ &\text{s.t. } \mathbf{F} \geq 0, \quad \mathbf{F}\mathbf{1}_R = \mathbf{1}_N\end{aligned} \tag{14}$$

where

$$S(\mathbf{F}) = \sum_{i=1}^{H}\gamma_i^P[\|\mathbf{U}^{(i)} - \mathbf{F}\mathbf{Z}^{(i)}\|_{2,1} + \beta Tr(\mathbf{F}^T\mathbf{L}^{(i)}\mathbf{F})]. \tag{15}$$

To effectively solve $\mathbf{F}$ with $\ell_{2,1}$-norm loss function, we introduce

$$\begin{aligned}J_1(\mathbf{F}) = \sum_{i=1}^{H}\gamma_i^P Tr\big[&\mathbf{U}^{(i)^T}\Lambda_4^{(i)}\mathbf{U}^{(i)} - 2\mathbf{U}^{(i)^T}\Lambda_4^{(i)}\mathbf{F}\mathbf{Z}^{(i)} \\ &+ \mathbf{Z}^{(i)^T}\mathbf{F}^T\Lambda_4^{(i)}\mathbf{F}\mathbf{Z}^{(i)} + \beta\mathbf{F}^T(\mathbf{D}^{(i)} - \mathbf{W}^{(i)})\mathbf{F}\big]\end{aligned} \tag{16}$$

where

$$\left(\Lambda_4^{(i)}\right)_{ll} = \frac{1}{2\|(\mathbf{U}^{(i)} - \mathbf{F}\mathbf{Z}^{(i)})_{l\cdot}\|}.$$

In order to cope with the ℓ_1 normalization constraint of $\mathbf{F}$, we introduce another variable $\widetilde{\mathbf{F}}$ and define $\mathbf{F}_{jk} = (\widetilde{\mathbf{F}}_{jk}/\sum_s\widetilde{\mathbf{F}}_{js})$. Then, we can optimize $J_1(\mathbf{F})$ by minimizing $J_2(\widetilde{\mathbf{F}})$, where

$$\begin{aligned}J_2(\widetilde{\mathbf{F}}) &= \sum_{i=1}^{H}\gamma_i^P \\ &\times\Bigg[Tr\left(\mathbf{U}^{(i)^T}\Lambda_4^{(i)}\mathbf{U}^{(i)}\right) - 2\sum_{jk}\left(\Lambda_4^{(i)}\mathbf{U}^{(i)}\mathbf{Z}^{(i)^T}\right)_{jk}\frac{\widetilde{\mathbf{F}}_{jk}}{\sum_s\widetilde{\mathbf{F}}_{js}} \\ &+ \sum_{jk}\left[\Lambda_4^{(i)}\left(\widetilde{\mathbf{F}} \oslash \left(\widetilde{\mathbf{F}}\mathbf{1}_R\mathbf{1}_R^T\right)\right)\mathbf{Z}^{(i)}\mathbf{Z}^{(i)^T}\right]_{jk}\frac{\widetilde{\mathbf{F}}_{jk}}{\sum_s\widetilde{\mathbf{F}}_{js}} \\ &+ \beta\sum_{jkl}\mathbf{D}_{jl}^{(i)}\frac{\widetilde{\mathbf{F}}_{jk}}{\sum_s\widetilde{\mathbf{F}}_{js}}\frac{\widetilde{\mathbf{F}}_{lk}}{\sum_s\widetilde{\mathbf{F}}_{ls}} - \beta\sum_{jkl}\mathbf{W}_{jl}^{(i)}\frac{\widetilde{\mathbf{F}}_{jk}}{\sum_s\widetilde{\mathbf{F}}_{js}}\frac{\widetilde{\mathbf{F}}_{lk}}{\sum_s\widetilde{\mathbf{F}}_{ls}}\Bigg].\end{aligned} \tag{17}$$

The auxiliary function [50] of $J_2(\widetilde{\mathbf{F}})$ can be constructed as

$$\begin{aligned}Z\left(\widetilde{\mathbf{F}}, \widetilde{\mathbf{F}}'\right) &= \sum_{i=1}^{H}\gamma_i^P \\ &\times\Bigg[Tr(\mathbf{U}^{(i)^T}\Lambda_4^{(i)}\mathbf{U}^{(i)}) - 2\sum_{jk}\left(\Lambda_4^{(i)}\mathbf{U}^{(i)}\mathbf{Z}^{(i)^T}\right)_{jk} \\ &\quad\times\frac{\widetilde{\mathbf{F}}'_{jk}}{\sum_s\widetilde{\mathbf{F}}'_{js}}\left(1 + \log\frac{\widetilde{\mathbf{F}}_{jk}/\sum_s\widetilde{\mathbf{F}}_{js}}{\widetilde{\mathbf{F}}'_{jk}/\sum_s\widetilde{\mathbf{F}}'_{js}}\right) \\ &\quad+ \sum_{jk}\left[\Lambda_4^{(i)}\left(\widetilde{\mathbf{F}}' \oslash \left(\widetilde{\mathbf{F}}'\mathbf{1}_R\mathbf{1}_R^T\right)\right)\mathbf{Z}^{(i)}\mathbf{Z}^{(i)^T}\right]_{jk} \\ &\quad\times\frac{(\widetilde{\mathbf{F}}_{jk}/\sum_s\widetilde{\mathbf{F}}_{js})^2}{\widetilde{\mathbf{F}}'_{jk}/\sum_s\widetilde{\mathbf{F}}'_{js}} \\ &\quad+ \beta\sum_{jk}\frac{\left[\mathbf{D}^{(i)}\left(\widetilde{\mathbf{F}}' \oslash \left(\widetilde{\mathbf{F}}'\mathbf{1}_R\mathbf{1}_R^T\right)\right)\right]_{jk}\left(\widetilde{\mathbf{F}}_{jk}/\sum_s\widetilde{\mathbf{F}}_{js}\right)^2}{\widetilde{\mathbf{F}}'_{jk}/\sum_s\widetilde{\mathbf{F}}'_{js}} \\ &\quad- \beta\sum_{jkl}\mathbf{W}_{jl}^{(i)}\frac{\widetilde{\mathbf{F}}'_{jk}}{\sum_s\widetilde{\mathbf{F}}'_{js}}\frac{\widetilde{\mathbf{F}}'_{lk}}{\sum_s\widetilde{\mathbf{F}}'_{ls}} \\ &\quad\times\left(1 + \log\frac{\left(\widetilde{\mathbf{F}}_{jk}/\sum_s\widetilde{\mathbf{F}}_{js}\right)\left(\widetilde{\mathbf{F}}_{lk}/\sum_s\widetilde{\mathbf{F}}_{ls}\right)}{\left(\widetilde{\mathbf{F}}'_{jk}/\sum_s\widetilde{\mathbf{F}}'_{js}\right)\left(\widetilde{\mathbf{F}}'_{lk}/\sum_s\widetilde{\mathbf{F}}'_{ls}\right)}\right)\Bigg].\end{aligned} \tag{18}$$

Setting the partial derivative of $\widetilde{\mathbf{F}}_{jk}$ to zero, we have

$$\frac{\partial Z(\widetilde{\mathbf{F}}, \widetilde{\mathbf{F}}')}{\widetilde{\mathbf{F}}_{jk}} = \sum_t\frac{\partial Z(\widetilde{\mathbf{F}}, \widetilde{\mathbf{F}}')}{\partial\left(\frac{\widetilde{\mathbf{F}}_{jt}}{\sum_s\widetilde{\mathbf{F}}_{js}}\right)}\frac{\partial\left(\frac{\widetilde{\mathbf{F}}_{jt}}{\sum_s\widetilde{\mathbf{F}}_{js}}\right)}{\partial\widetilde{\mathbf{F}}_{jk}} = 0. \tag{19}$$

Algorithm 1 Computing the Fixed Point of (22)

```
Input: $\Gamma$, $\Theta$, $\mathbf{F}$, $MaxIter$
Output: $\mathbf{F}$
while not converged do
    $\Psi = (\Gamma - \Theta \odot \mathbf{F}^2)\mathbf{1}_R\mathbf{1}_R^T$;
    $\mathbf{F} = (\sqrt{\Psi^2 + 4\Theta\Gamma} - \Psi) \oslash (2\Theta)$;
    $\mathcal{I} = \{i | \Psi_{i1} < 0\}$;
    if $\mathcal{I}$ is not empty then
        $\mathbf{F}_{\mathcal{I}\cdot} \leftarrow diag(\mathbf{F}_{\mathcal{I}\cdot}\mathbf{1}_R)^{-1}\mathbf{F}_{\mathcal{I}\cdot}$;
    end
end
```

By replacing $((\widetilde{\mathbf{F}}_{jt})/(\sum_s \widetilde{\mathbf{F}}_{js})) = \mathbf{F}_{jt}$, we can obtain

$$\frac{\partial Z(\widetilde{\mathbf{F}}, \widetilde{\mathbf{F}}')}{\partial\left(\frac{\widetilde{\mathbf{F}}_{jt}}{\sum_s \widetilde{\mathbf{F}}_{js}}\right)} = \sum_{i=1}^{H} \gamma_i^P \times \Bigg[-2\big(\Lambda_4^{(i)}\mathbf{U}^{(i)}\mathbf{Z}^{(i)^T}\big)_{jt}\frac{\mathbf{F}'_{jt}}{\mathbf{F}_{jt}} + 2\big(\Lambda_4^{(i)}\mathbf{F}'\mathbf{Z}^{(i)}\mathbf{Z}^{(i)^T}\big)_{jt}\frac{\mathbf{F}_{jt}}{\mathbf{F}'_{jt}} + \frac{2\beta(\mathbf{D}^{(i)}\mathbf{F}')_{jt}\mathbf{F}_{jt}}{\mathbf{F}'_{jt}} - \frac{2\beta(\mathbf{W}^{(i)}\mathbf{F}')_{jt}\mathbf{F}'_{jt}}{\mathbf{F}_{jt}}\Bigg]. \quad (20)$$

In addition, we have

$$\frac{\partial\left(\frac{\widetilde{\mathbf{F}}_{jt}}{\sum_s \widetilde{\mathbf{F}}_{js}}\right)}{\partial \widetilde{\mathbf{F}}_{jk}} = \frac{\delta_{kt} - \mathbf{F}_{jt}}{\sum_s \widetilde{\mathbf{F}}_{js}}, \quad \delta_{tk} = \begin{cases} 1 & \text{if } t = k \\ 0 & \text{otherwise.} \end{cases} \quad (21)$$

Let $\Gamma = [\sum_{i=1}^{H} \gamma_i^P (\Lambda_4^{(i)}\mathbf{U}^{(i)}\mathbf{Z}^{(i)^T} + \beta\mathbf{W}^{(i)}\mathbf{F}')] \odot \mathbf{F}'$ and $\Theta = [\sum_{i=1}^{H} \gamma_i^P (\Lambda_4^{(i)}\mathbf{F}'\mathbf{Z}^{(i)}\mathbf{Z}^{(i)^T} + \beta\mathbf{D}^{(i)}\mathbf{F}')] \oslash \mathbf{F}'$, then, (19) can be written as

$$\Theta_{jk}\mathbf{F}_{jk}^2 + \sum_s \big[\Gamma_{js} - \Theta_{js}\mathbf{F}_{js}^2\big]\mathbf{F}_{jk} - \Gamma_{jk} = 0. \quad (22)$$

By summing (22) over k, we obtain

$$\sum_k \Theta_{jk}\mathbf{F}_{jk}^2 + \sum_s \big[\Gamma_{js} - \Theta_{js}\mathbf{F}_{js}^2\big]\sum_k \mathbf{F}_{jk} - \sum_k \Gamma_{jk} = \sum_s \big[\Gamma_{js} - \Theta_{js}\mathbf{F}_{js}^2\big]\left(\sum_k \mathbf{F}_{jk} - 1\right) = 0 \quad (23)$$

where we can observe that the solution of (23) always satisfies ℓ_1 normalization for almost all β. To obtain $\mathbf{F}$, we compute the fixed point of (22) by Algorithm 1, which is developed in [42] and [43]. The convergence of Algorithm 1 has been proved in [42] and only a few iterations are needed to converge (always less than ten iterations in our experiments).

C. Update γ_i

Using Lagrange multiplier method, we can derive the following updating rule for γ_i.

If $P > 1$

$$\gamma_i = 1\Bigg/{\sum_{j=1}^{H} (\Delta^{(i)}/\Delta^{(j)})}^{1/(P-1)}. \quad (24)$$

For $P = 1$ case, we have

$$\gamma_i = \begin{cases} 1, & i = \text{argmin}_i\, \Delta^{(i)} \\ 0, & \text{otherwise} \end{cases} \quad (25)$$

where $\Delta^{(i)} = \|\mathbf{U}^{(i)} - \mathbf{F}\mathbf{Z}^{(i)}\|_{2,1} + \beta Tr(\mathbf{F}^T\mathbf{L}^{(i)}\mathbf{F})$.

D. Convergence Analysis

In each iteration, BLMV needs to update all the variables $\gamma_i, \mathbf{U}^{(i)}, \mathbf{V}^{(i)}, \mathbf{F}$, and $\mathbf{Z}^{(i)}$. It is obvious that the lower bound of objective function $\mathcal{O}_U$ in (6) is zero. To prove the convergence of the updating rules, we need to show that $\mathcal{O}_U$ is nonincreasing under each updating step. Since the solution for γ_i is obtained by Lagrange multiplier method, the objective is nonincreasing after updating and it is convergent. For the other variables $\mathbf{U}^{(i)}, \mathbf{V}^{(i)}, \mathbf{F}$, and $\mathbf{Z}^{(i)}$, we make use of auxiliary function method [8] to prove the convergence. The detailed proof of the convergence of updating $\mathbf{F}$ is provided, and we skip the proofs with respect to $\mathbf{U}^{(i)}, \mathbf{V}^{(i)}$, and $\mathbf{Z}^{(i)}$, since they are similar in spirit to the proof with respect to $\mathbf{F}$.

First, we introduce the following lemma, and then the convergence is proved in Theorem 1.

Lemma 1: In each update of $\mathbf{F}$, the following inequation holds:

$$\begin{aligned} &S(\mathbf{F}^{t+1}) - S(\mathbf{F}^t) \\ &\le \sum_{i=1}^{H} \gamma_i^P \big\{Tr[(\mathbf{U}^{(i)} - \mathbf{F}^{t+1}\mathbf{Z}^{(i)})^T\Lambda_4^{(i)}(\mathbf{U}^{(i)} - \mathbf{F}^{t+1}\mathbf{Z}^{(i)})] \\ &\quad + \beta Tr(\mathbf{F}^{t+1^T}\mathbf{L}^{(i)}\mathbf{F}^{t+1}) - Tr[(\mathbf{U}^{(i)} - \mathbf{F}^t\mathbf{Z}^{(i)})^T \\ &\quad \times \Lambda_4^{(i)}(\mathbf{U}^{(i)} - \mathbf{F}^t\mathbf{Z}^{(i)})] - \beta Tr(\mathbf{F}^{t^T}\mathbf{L}^{(i)}\mathbf{F}^t)\big\} \end{aligned} \quad (26)$$

where

$$\big(\Lambda_4^{(i)}\big)_{ll} = \frac{1}{2\|(\mathbf{U}^{(i)} - \mathbf{F}^t\mathbf{Z}^{(i)})_{l\cdot}\|}.$$

Proof:

$$\begin{aligned} &S(\mathbf{F}^{t+1}) - S(\mathbf{F}^t) \\ &= \sum_{i=1}^{H} \gamma_i^P \big[\|\mathbf{U}^{(i)} - \mathbf{F}^{t+1}\mathbf{Z}^{(i)}\|_{2,1} + \beta Tr(\mathbf{F}^{t+1^T}\mathbf{L}^{(i)}\mathbf{F}^{t+1}) \\ &\quad - \|\mathbf{U}^{(i)} - \mathbf{F}^t\mathbf{Z}^{(i)}\|_{2,1} - \beta Tr(\mathbf{F}^{t^T}\mathbf{L}^{(i)}\mathbf{F}^t)\big]. \end{aligned} \quad (27)$$

Comparing (27) with the right-hand side of (26), we only need to prove that the following inequality holds:

$$\begin{aligned} &\sum_{i=1}^{H} \gamma_i^P [\|\mathbf{U}^{(i)} - \mathbf{F}^{t+1}\mathbf{Z}^{(i)}\|_{2,1} - \|\mathbf{U}^{(i)} - \mathbf{F}^t\mathbf{Z}^{(i)}\|_{2,1}] \\ &\le \sum_{i=1}^{H} \gamma_i^P \big\{Tr[(\mathbf{U}^{(i)} - \mathbf{F}^{t+1}\mathbf{Z}^{(i)})^T\Lambda_4^{(i)}(\mathbf{U}^{(i)} - \mathbf{F}^{t+1}\mathbf{Z}^{(i)})] \\ &\quad - Tr[(\mathbf{U}^{(i)} - \mathbf{F}^t\mathbf{Z}^{(i)})^T\Lambda_4^{(i)}(\mathbf{U}^{(i)} - \mathbf{F}^t\mathbf{Z}^{(i)})]\big\}. \end{aligned} \quad (28)$$

It is obvious to prove the above inequation by a similar inequation, which is given by [46, Lemma 3]. □

Theorem 1: The objective function $\mathcal{O}_U$ in (6) is nonincreasing after updating $\mathbf{F}$.

Algorithm 2 Algorithm of BLMV

```
Input: Multi-view data matrices $\mathcal{X} = \{\mathbf{X}^{(i)}\}_{i=1}^{H}$, graph
       Laplacians $\mathbf{L}^{(h)} = \mathbf{D}^{(h)} - \mathbf{W}^{(h)}, \forall i = 1, \ldots, H$
       and parameters: $\lambda, \eta, \beta, P, \theta, K, R$
Output: The compact representation $\mathbf{F}$
Initialize $\{\mathbf{U}^{(i)}, \mathbf{V}^{(i)}, \mathbf{Z}^{(i)}\}_{i=1}^{H}, \mathbf{F}$ with non-negative values,
and let $\gamma_i = \frac{1}{H}, \forall i = 1, \ldots, H$
while not converged do
    for $i = 1$ to $H$ do
        Update $\mathbf{U}_S^{(i)}$ and $\mathbf{U}_P^{(i)}$ by equation (9) and (10);
        Update $\mathbf{V}_S^{(i)}$ and $\mathbf{V}_P^{(i)}$ by equation (11) and (12);
    end
    for $i = 1$ to $H$ do
        Update $\mathbf{Z}^{(i)}$ by equation (13);
    end
    Compute $\Gamma$ and $\Theta$;
    Update $\mathbf{F}$ by Algorithm 1;
    Update $\gamma_i, \forall i = 1, \ldots, H$ by equation (24) and (25);
end
```

Proof: Based on the properties of the auxiliary function, we have $J_1(\mathbf{F}^{t+1}) \le Z(\mathbf{F}^{t+1}, \mathbf{F}^t) \le Z(\mathbf{F}^t, \mathbf{F}^t) = J_1(\mathbf{F}^t)$. Thus, $J_1(F)$ will monotonically decrease under the update of $\mathbf{F}$, so we have $J_1(\mathbf{F}^{t+1}) \le J_1(\mathbf{F}^t)$, that is

$$\begin{aligned}\sum_{i=1}^{H} \gamma_i^P \{&Tr[(\mathbf{U}^{(i)} - \mathbf{F}^{t+1}\mathbf{Z}^{(i)})^T \Lambda_4^{(i)} (\mathbf{U}^{(i)} - \mathbf{F}^{t+1}\mathbf{Z}^{(i)})] \\ &+ \beta Tr(\mathbf{F}^{t+1^T}\mathbf{L}^{(i)}\mathbf{F}^{t+1})\} \\ \le \sum_{i=1}^{H} \gamma_i^P \{&Tr[(\mathbf{U}^{(i)} - \mathbf{F}^{t}\mathbf{Z}^{(i)})^T \Lambda_4^{(i)} (\mathbf{U}^{(i)} - \mathbf{F}^{t}\mathbf{Z}^{(i)})] \\ &+ \beta Tr(\mathbf{F}^{t^T}\mathbf{L}^{(i)}\mathbf{F}^{t})\} \end{aligned} \tag{29}$$

where $(\Lambda_4^{(i)})_{ll} = (1/(2\|(\mathbf{U}^{(i)} - \mathbf{F}^t\mathbf{Z}^{(i)})_{l\cdot}\|))$.

According to Lemma 1, we have $S(\mathbf{F}^{t+1}) - S(\mathbf{F}^t) \le 0$. This proves that the objective function $\mathcal{O}_U$ in (6) is nonincreasing after updating $\mathbf{F}$ in each iteration. □

E. Computational Complexity Analysis

Before updating each variable of BLMV, the nearest neighbor graphs are constructed for different views. We need $O(N^2 M_i)$ to construct these graphs. During the updating process of BLMV, we calculate the computational cost in each iteration based on updating rules. It should be noted that the p-nearest neighbor graphs $\{\mathbf{W}^{(i)}\}_{i=1}^{H}$ are highly sparse matrices. Therefore, the computational cost to calculate $\mathbf{W}^{(i)}\mathbf{F}$ is only $O(pNR)$. The overall computational complexities for each variable are: $O(NM_iK)$ for updating $\mathbf{U}^{(i)}$ and $\mathbf{V}^{(i)}$, and $O(NKR)$ for updating $\mathbf{F}$ and $\mathbf{Z}^{(i)}$, where N is the number of samples, M_i, K, and R are the dimensionality of the ith view, the comparable representation, and the compact representation, respectively. The computational cost of the updating process is comparable with that of standard NMF; therefore, our method is efficient.

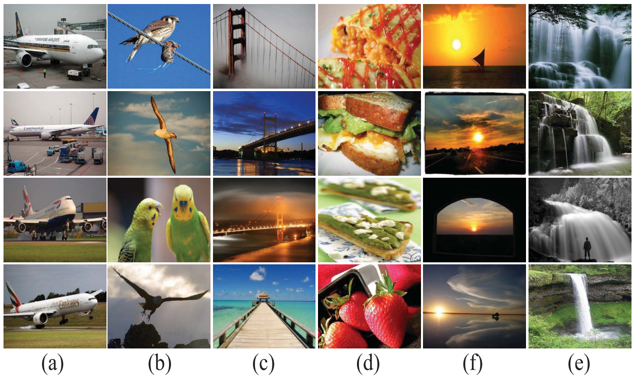
(a) (b) (c) (d) (f) (e)

Fig. 2. Some example images from NUS-WIDE data set. (a) Airport. (b) Bird. (c) Bridge. (d) Food. (e) Sunset. (f) Waterfall.

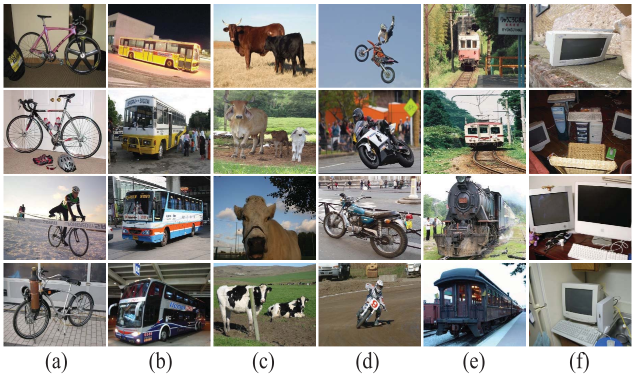
(a) (b) (c) (d) (e) (f)

Fig. 3. Some example images from PASCAL VOC data set. (a) Bicycle. (b) Bus. (c) Cow. (d) Motorbike. (e) Train. (f) TV monitor.

V. Experimental Results

To verify the effectiveness of the proposed method BLMV, we investigate its performance in the tasks of image classification and annotation on two benchmark real-world image data sets. Our method is compared with several representative multiview learning methods to demonstrate its effectiveness. First, we introduce the data sets, the compared methods, and experimental settings. Then, we present the image classification and annotation performance of the proposed method and the other methods. Finally, a parameter sensitivity analysis is provided to illustrate the properties of BLMV.

A. Data Sets

Two real-world image data sets NUS-WIDE (NUS) [51] and PASCAL VOC'07 (VOC) [52] are adopted in our experiments. NUS is a web image data set and it includes 269 648 images and associated tags from Flickr. There are 81 ground truth labels that can be used for evaluation. VOC data set contains around 10 000 images obtained from Flickr web site and all of them are annotated for 20 categories. Some example images from the two data sets are shown in Figs. 2 and 3, respectively.

From each of the two data sets, we randomly sample 6000 images as our data sets. Five different visual features are extracted as five views of image data. These visual features and their dimensionalities are blockwise color moments (729) [53], bag of visual words based on scale-invariant feature transform (SIFT) (1000) [54], histogram of gradient (HOG) (3100) [55], GIST (512) [56], and local binary patterns (LBPs) (928) [57].

B. Compared Methods

To demonstrate the effectiveness of BLMV, we learn the low-dimensional representation by several compared methods, including two traditional PCA-based methods (1 and 2), six recently proposed multiview learning methods (3–8), and two versions of our model with different settings (9, and 10).

1) *Single View PCA (sPCA):* Perform PCA for each view to obtain the low-dimensional representation and report the results with best performance.
2) *Multiview PCA:* Concatenate each view together and then perform PCA to obtain the low-dimensional representation.
3) *Multiview Spectral Embedding (MVSE):* A spectral embedding method for multiview dimensionality reduction proposed in [1].
4) *Multifeature Spectral Clustering With Minimax Optimization (MSCMO):* A multiview spectral clustering method [58] and the learned feature embedding are used as the low-dimensional representation.
5) *Group Sparse Multiview Patch Alignment Framework:* A joint multiview feature extraction and feature selection method [21] based on patch alignment.
6) *Sparse Dimensionality Reduction for Multiview Data (SSMVD):* A multiview dimensionality reduction method [5] based on structured sparse PCA which improves flexibility in sharing information across different views.
7) *Ensemble Manifold Regularized Sparse Low-Rank Approximation (EMRSLRA):* A multiview feature embedding method [40] that based on least-squares component analysis and ensemble manifold learning.
8) *Coregularized NMF (CoNMF):* An NMF-based multiview clustering method [49]. The learned coefficient matrix is used as the low-dimensional representation. Both pairwise and clusterwise CoNMF are performed and the best results are reported.
9) *BLMV Without the First Level (BLMV_SL):* Let $\mathbf{X}^{(i)}$ instead of $\mathbf{U}^{(i)}$ to feed into the second level of BLMV. This method is to validate that the proposed bilevel learning strategy can more effectively leverage the multiview complementary information.
10) *BLMV Using Frobenius Norm (BLMV_F):* Replace $\ell_{2,1}$-norm with F-norm in the second level of BLMV. This baseline is used to test how our method (with $\ell_{2,1}$-norm) is resistent to noise and outliers.

C. Evaluation Metrics

To evaluate the image classification and annotation performance, we adopt the three criteria, as adopted in [5]: accuracy (ACC), the area under the receiver operating characteristics curve (AUC), and F1 (F-measure) scores. They are typical evaluation metrics for the tasks of image classification and annotation.

ACC is defined as ACC=N_r/N_t, where N_t is the total number of test images to be labeled and N_r is the number of images that are annotated with right labels or correctly classified. The detailed definition of AUC and F1 scores can be referred to [59].

TABLE I

IMAGE CLASSIFICATION AND ANNOTATION COMPARISON ON DIFFERENT DATA SETS. (a) PERFORMANCE COMPARISON ON NUS DATA SET. (b) PERFORMANCE COMPARISON ON VOC DATA SET

(a)

Method	ACC Score	AUC Score	F1 Score
sPCA	0.669 ± 0.004	0.744 ± 0.005	0.303 ± 0.004
mPCA	0.707 ± 0.007	0.791 ± 0.003	0.345 ± 0.003
MVSE	0.701 ± 0.012	0.749 ± 0.003	0.317 ± 0.006
MSCMO	0.716 ± 0.010	0.758 ± 0.004	0.330 ± 0.003
GSMVPA	0.696 ± 0.006	0.780 ± 0.003	0.336 ± 0.004
SSMVD	0.710 ± 0.005	0.793 ± 0.003	0.348 ± 0.004
EMRSLRA	0.700 ± 0.006	0.792 ± 0.002	0.343 ± 0.004
CoNMF	0.699 ± 0.014	0.793 ± 0.008	0.343 ± 0.005
BLMV_SL	0.724 ± 0.013	0.788 ± 0.008	0.349 ± 0.007
BLMV_F	0.717 ± 0.010	0.797 ± 0.006	0.354 ± 0.005
BLMV	$\mathbf{0.737 \pm 0.007}$	$\mathbf{0.803 \pm 0.006}$	$\mathbf{0.363 \pm 0.006}$

(b)

Method	ACC Score	AUC Score	F1 Score
sPCA	0.816 ± 0.011	0.754 ± 0.007	0.224 ± 0.005
mPCA	0.827 ± 0.006	0.786 ± 0.003	0.247 ± 0.004
MVSE	0.823 ± 0.005	0.748 ± 0.004	0.223 ± 0.004
MSCMO	0.830 ± 0.009	0.756 ± 0.006	0.232 ± 0.004
GSMVPA	0.845 ± 0.010	0.777 ± 0.007	0.251 ± 0.003
SSMVD	0.849 ± 0.006	0.794 ± 0.003	0.268 ± 0.002
EMRSLRA	0.840 ± 0.005	0.793 ± 0.004	0.263 ± 0.005
CoNMF	0.859 ± 0.007	0.777 ± 0.003	0.254 ± 0.003
BLMV_SL	0.871 ± 0.008	0.778 ± 0.005	0.269 ± 0.005
BLMV_F	0.873 ± 0.006	0.786 ± 0.003	0.277 ± 0.006
BLMV	$\mathbf{0.886 \pm 0.005}$	$\mathbf{0.804 \pm 0.004}$	$\mathbf{0.297 \pm 0.006}$

D. Experimental Setting

We evaluate the effectiveness of low-dimensional representation learned by BLMV in the tasks of image classification and annotation. Specifically, all the multiview data are first embedded into a low-dimensional space by using both the compared methods and BLMV. Then, we conduct image classification in this space based on linear support vector machines (SVMs). The one-against-the-rest scheme is adopted, where one classifier is trained for each category. For all the methods, we learn the low-dimensional representation with different dimensionalities $R = \{50, 100, 150, 200, 250, 300, 350, 400\}$, and then image classification is conducted for each R. Higher classification performance indicates that more effective low-dimensional representation is obtained. We randomly partition the data set into training set and test set ten times, and the averaged performance is reported.

The parameters of the compared methods are set as suggested in their works. There are several parameters in our method BLMV. To model the geometric structure of image data, we construct a seven-NN graph for each view and the corresponding graph Laplacian matrix. The Gaussian kernel width parameter σ is estimated by the average of the pairwise distances. For the rest of the parameters, we determine them by cross validation. In the first random partition of training and test set, the training set is split into five folds. Then, we tune the parameters by five-fold cross-validation and choose the

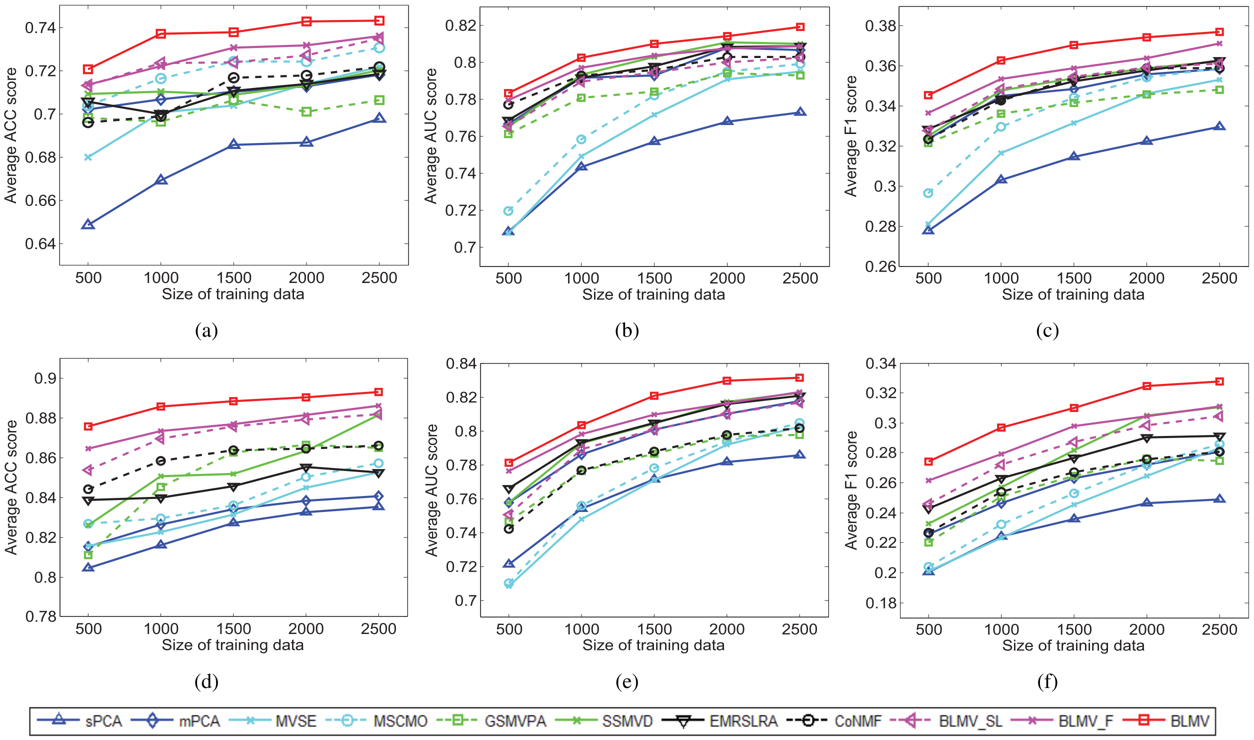

(a) (b) (c)

(d) (e) (f)

Fig. 4. Performance comparison of image classification and annotation with different numbers of training data on NUS and VOC data sets. The size of training set varies in the range of {500, 1000, 1500, 2000, 2500} and R is fixed to 100. (a) ACC on NUS. (b) AUC on NUS. (c) F1 on NUS. (d) ACC on VOC. (e) AUC on VOC. (f) F1 on VOC.

parameter settings with the best average performance. These parameter settings are used for training and testing. Thus, we set $\lambda = 1$, $\eta = 1$, $P = 2$, $\theta = 0.75$, $K = 400$, and $\beta = 1e-4$ for NUS and VOC data set in our experiments. To further illustrate the properties of these parameters, we will present the detailed parameter sensitivity analysis in Section V-F.

E. Results Analysis

We first test image classification and annotation performance with dimensionality $R = 100$, and we randomly select 1000 images as training set and the rest images are used for testing. The mean and standard errors of image classification and annotation performance on NUS and VOC data sets are listed in Table I. It is obvious that the BLMV achieves the best image classification and annotation performance compared with the other methods on both data sets, which demonstrates the effectiveness of our method in multiview low-dimensional representation learning. Compared with the best results obtained by the other methods, our method achieves improvement of 2.1% in ACC, 1.0% in AUC, 1.5% in F1 score for NUS data set, 2.7% in ACC, 1.0% in AUC, and 2.9% in F1 score for VOC data set.

Moreover, we conduct experiments with a different size of training set and fix $R = 100$. The size of training set is set to be {500, 1000, 1500, 2000, 2500}, and the detailed performance is shown in Fig. 4. It can be clearly observed that as we use more data for training classifiers, the performance of each method improves stably. Compared with the other methods, BLMV achieves the best performance with different number of training data, which indicates that the low-dimensional representation obtained by BLMV is more discriminative and effective than that obtained by the other methods.

To further demonstrate the performance improvement of our method compared with the other methods in image classification and annotation, we conduct image classification and annotation experiments at different dimensionalities $R = \{50, 100, \ldots, 400\}$; 1000 images are used for training and the rest are used for testing. Fig. 5 shows the detailed experimental results. We can observe that the two spectral embedding methods, MVSE and MSCMO, usually achieve their best performance at lower dimensions, and the performance degraded as the dimension increasing. This is because the learned basis by these two methods is orthogonal and the first few dimensions may have high variance and they are quite discriminative. However, the variance of basis becomes lower and lower as the dimension increases, so the representation becomes ambiguous and meaningless, since it is dominated by these low discriminative dimensions. On the other hand, some latent space-based methods, such as SSMVD, CONMF, and BLMV, achieve better performance at higher dimensions. This is reasonable, because more information can be preserved with more latent factors. Compared with the other methods, BLMV generally achieves better performance at different dimensions. In particular, BLMV obtains relatively stable performance when $R > 50$, which indicates that its performance is not sensitive to R, and BLMV can effectively encode the multiview information at a wide range of dimension settings.

Throughout the experiments, we reveal several interesting points as follows.

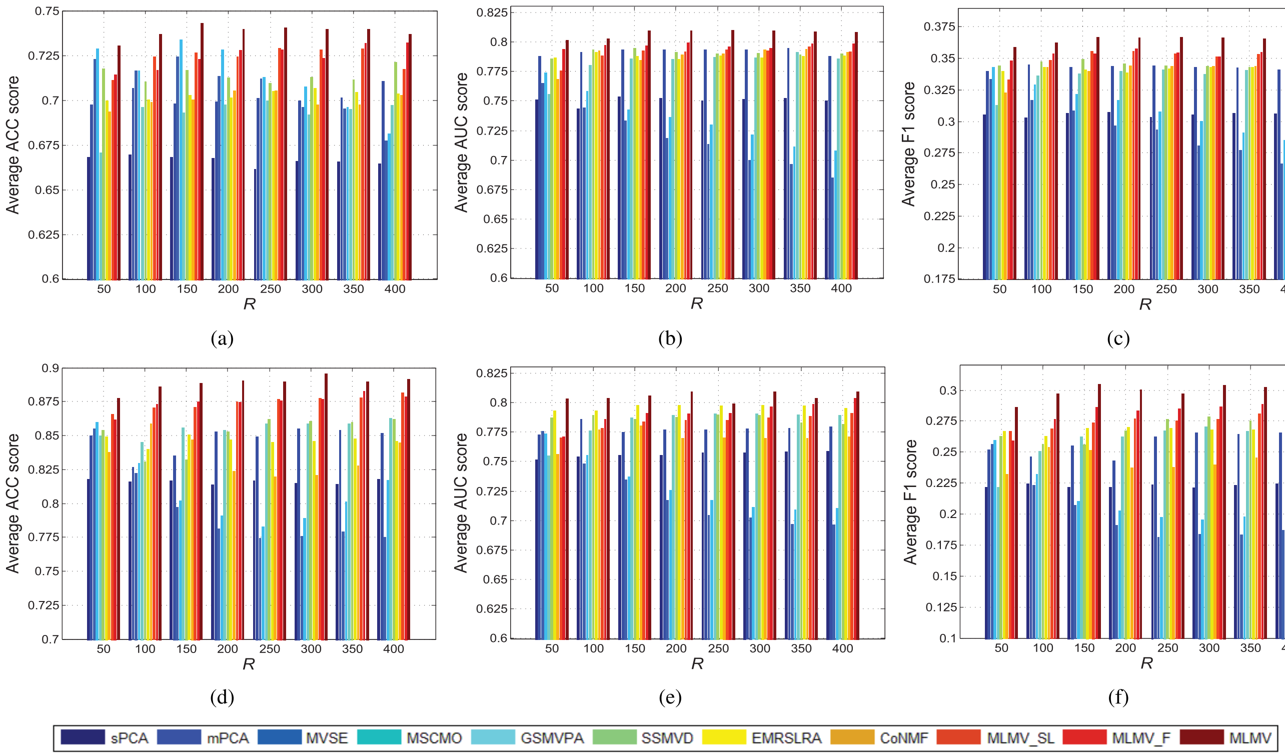

(a) (b) (c)

(d) (e) (f)

Fig. 5. Performance comparison of image classification and annotation with different dimensionalities $R = \{50, 100, \ldots, 400\}$. The size of training data is set to 1000. (a) ACC on NUS. (b) AUC on NUS. (c) F1 on NUS. (d) ACC on VOC. (e) AUC on VOC. (f) F1 on VOC.

1) All the multiview dimensionality reduction methods are superior to the single-view-based method sPCA. This indicates that exploiting multiple views can generate a more powerful description than only using a single view.
2) From the performance comparison between two MVSE methods MVSE and MSCMO, we can find that by considering the different importance of views and minimizing pairwise disagreement between any two views, MSCMO learns a more harmonic consensus representation. Therefore, it fuses multiview information more effectively and achieves better performance than MVSE.
3) Compared with EMRSLRA, BLMV can more effectively conduct multiview fusion. It learns nonnegative latent spaces, which are naturally interpretable, so that different views with different physical meanings are comparable. Besides, by assigning different weights to multiple views during multiview matrix factorization, BLMV can accommodate unreliable views and obtain more accurate results than EMRSLRA.
4) BLMV outperforms another nonnegative latent space learning method CoNMF. CoNMF only regularizes the coefficient matrices of different views toward a consensus, whereas BLMV simultaneously utilizes the shared and the private nature as well as the intrinsic geometric structure information of multiview data, which helps to obtain a more compact and discriminative low-dimensional representation.
5) BLMV_SL performs unsatisfactorily, because it directly learns the low-dimensional representation from heterogeneous multiview features, which ignores the incomparability of different views. In addition, neither shared nor private information of multiview data can be well captured by BLMV_SL so that its overall performance is limited. The experimental results of BLMV_SL illustrate that the comparable representation

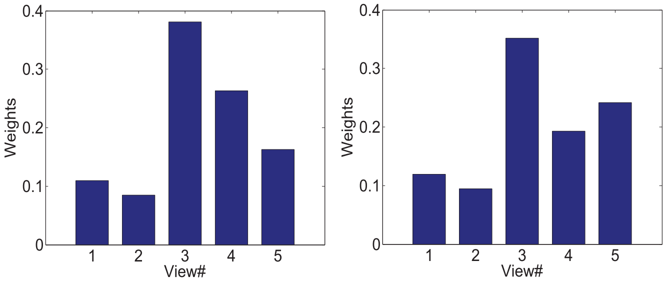

(a) (b)

Fig. 6. Learned weights γ_i on each data set. View 1 to view 5 represent color moments, GIST, HOG, SIFT, and LBP features, respectively. (a) NUS. (b) VOC.

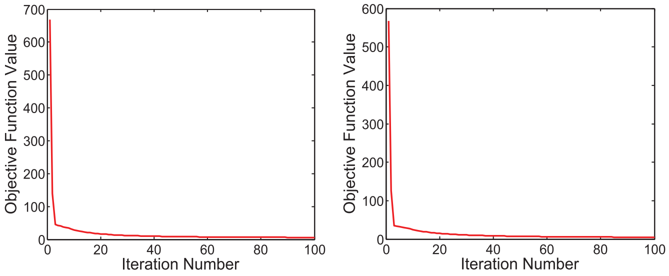

(a) (b)

Fig. 7. Convergence curves of BLMV over NUS and VOC data sets. (a) Convergence curve on NUS. (b) Convergence curve on VOC.

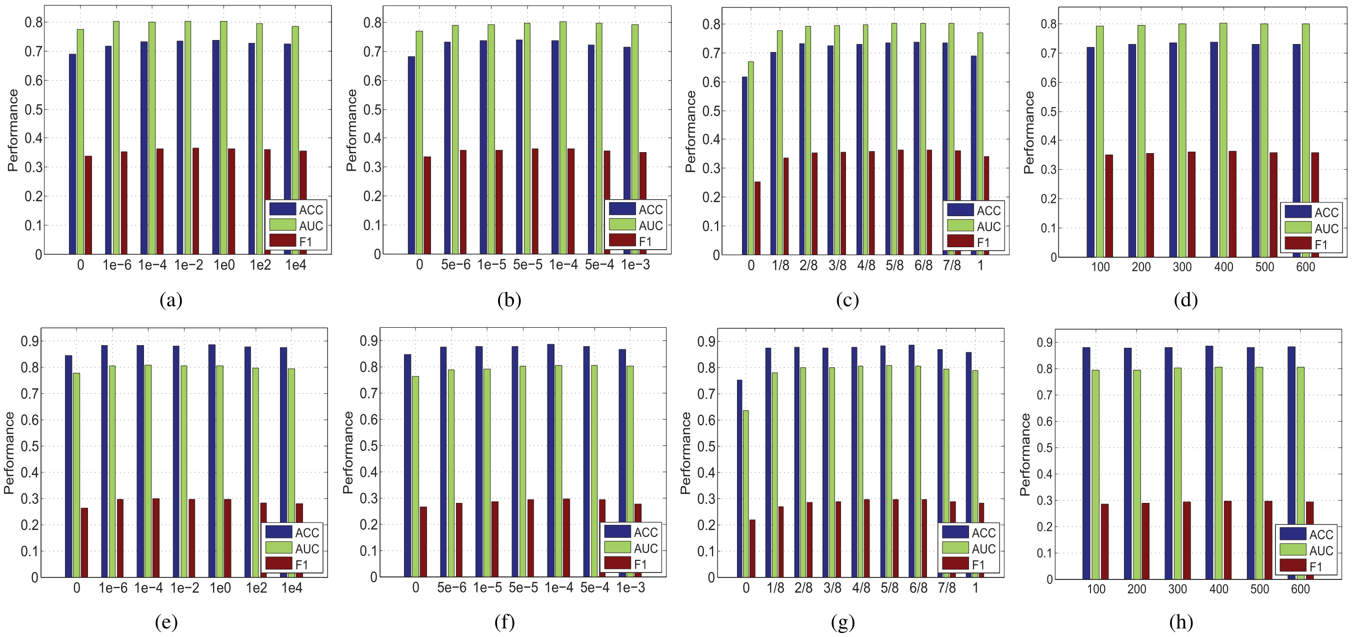

Fig. 8. Parameter sensitivity analysis on NUS and VOC data sets. The averaged performance of BLMV with different values of the four parameters λ, β, θ, and K on NUS and VOC data sets is illustrated. (a) Vary λ on NUS. (b) Vary β on NUS. (c) Vary θ on NUS. (d) Vary K on NUS. (e) Vary λ on VOC. (f) Vary β on VOC. (g) Vary θ on VOC. (h) Vary K on VOC.

learning helps to accurately capture the information of each view and further enhances the effectiveness of compact representation. The proposed bilevel learning strategy is both reasonable and efficient for multiview representation learning.

6) BLMV further improves the image classification performance compared with BLMV_F, which demonstrates that the adopted $\ell_{2,1}$-norm in the second level is capable of resisting the outliers and noise contained in the multiview data and provides more accurate and reliable learning results. Specifically, compared with BLMV_F from Table I, BLMV gains 2.0%, 0.6%, and 0.9% improvement in terms of ACC, AUC, and F1 scores on NUS data set and it also gains 1.3%, 1.8%, and 2.0% improvement in terms of ACC, AUC, and F1 scores on VOC data set.

Next, we illustrate the weight of each view γ_i learned by BLMV and analyze the different importance of views. The detailed weights are shown in Fig. 6. We can observe that the weights learned from the two data sets share similar distribution properties, i.e., HOG, SIFT, and LBP obtain higher weights than color moments and GIST. This indicates that the images from the two real-world data sets have similar visual appearance, and using the local features, such as HOG, SIFT, and LBP, can achieve better discrimination results. Color moments and GIST are relatively unreliable, since they obtain lower weights. HOG, SIFT, and LBP generate more accurate descriptions so that they are more important for multiview dimensionality reduction.

In the end, the convergence curves of the two data sets are shown in Fig. 7, where we can see that the objective function value is nonincreasing after each iteration. Fig. 7 indicates that the proposed optimization algorithm can effectively solve the objective function and converges quickly.

F. Parameter Sensitivity Analysis

There are four critical parameters λ, β, θ, and K in BLMV. λ controls the consistency of the shared parts of each view. β measures the strength of encoding the intrinsic geometric structure into the low-dimensional representation. θ controls the proportion of shared parts and private parts in comparable representation learning. K is the dimensionality of comparable representation. To analysis the property of each parameter, we use the same parameter settings that are obtained by cross validation, as introduced in Section V-D, and then vary one at a time while fixing the others to see the performance variations. The number of training data is set to 1000 and the dimensionality of compact representation R is set to 100. The averaged performance on NUS and VOC data sets is reported in Fig. 8.

First, we vary λ in the range of $\{0, 1e-6, 1e-4, \ldots, 1e4\}$ and the results are shown in Fig. 8(a) and (e). The performance of BLMV is not good when $\lambda = 0$. Because no consistent constraints are imposed on the shared parts of each view, the views cannot complement with each other well. Then, as λ becomes larger, different views can share the information with each other and BLMV achieves good performance in the range of $[1e-4, 1e2]$ on both data sets. Nevertheless, the performance of BLMV degrades slightly when λ becomes too large ($\lambda = 1e4$). This is mainly due to the shared parts that are highly consistent with each other under this condition so that the original properties of each view cannot be well preserved. In general, the performance of BLMV is not sensitive to parameter λ in a wide range of $[1e{-}4, 1e2]$, which can provide satisfied results.

Then, we investigate the influence of parameter β in BLMV. From Fig. 8(b) and (f), we observe that good image classification and annotation results can be obtained when $\beta \in [5e-6, 1e-4]$ for NUS data set and $\beta \in [5e-5, 5e-4]$

for VOC data set. When $\beta = 0$, no structure information is encoded in the low-dimensional representation so that the performance of BLMV is unsatisfied. As β becomes larger, more and more structure information are preserved and the performance is improved accordingly. This variation tendency demonstrates that the nonlinearity inherent in multiview data is important, and considering such an intrinsic structure can make the learned low-dimensional representation more compact and discriminative. In addition, when β is set to a large value of $1e-3$, the performance is degraded slightly, since the learned representation is affected by such excessive regularization. Similar to λ, the overall performance will not be greatly influenced by varying β in a wide range of $[5e-6, 5e-4]$.

Fig. 8(c) and (g) illustrates how the performance varies with parameter θ. For NUS and VOC data set, the satisfied performance can be achieved when $\theta \in [3/8, 6/8]$ and [2/8, 6/8], respectively. The shared information cannot be well encoded when $\theta \leq 1/8$ and the private information of each view is not fully captured for $\theta > 7/8$. BLMV cannot generate satisfied performance in both cases. It indicates that exploiting the shared and the private nature of multiview data will help BLMV accurately capturing the information of each view and better utilizing the complementary information, which improves the performance of learning tasks.

Finally, we investigate the performance of BLMV with different K values. From Fig. 8(d) and (h), we observe that good performance is achieved on both NUS and VOC data sets by our method when K is around 400. The performance is limited when $K < 200$, since there are not enough latent factors to fully encode the multiview information. The appropriate results can be obtained for $K > 200$, where BLMV is not sensitive to the variation of K, because the number of latent factors is capable of sufficiently preserving the information of each view.

VI. Conclusion

In this paper, we propose an unsupervised multiview dimensionality reduction method for image data, which is based on bilevel latent space learning. The first level aims to learn the comparable representation from multiple views with different physical meanings. Both shared and independent parts of each view are explored to accurately represent the information of each view. In the second level, we adopt a robust loss function and preserve the intrinsic manifold structure of images, which guarantees the learned representation to be more reliable and discriminative. By introducing the bilevel learning strategy, our method possesses more powerful abilities to leverage the complementary nature of multiview data and generates promising results. An efficient iterative algorithm is also developed to solve the objective function. Image classification and annotation experiments conducted on two real-world data sets demonstrate the effectiveness of the proposed method. In our future work, we will find a smarter way to determine the parameters in our method. Moreover, we expect to exploit the category information and generalize the method to supervised learning tasks, so that a more discriminative and semantically consistent low-dimensional representation can be obtained.

References

[1] B. Long, P. S. Yu, and Z. Zhang, "A general model for multiple view unsupervised learning," in *Proc. SDM*, 2008, pp. 822–833.

[2] T. Xia, D. Tao, T. Mei, and Y. Zhang, "Multiview spectral embedding," *IEEE Trans. Syst., Man, Cybern. B, Cybern.*, vol. 40, no. 6, pp. 1438–1446, Dec. 2010.

[3] A. Kumar, P. Rai, and H. Daume, "Co-regularized multi-view spectral clustering," in *Proc. Adv. Neural Inf. Process. Syst.*, 2011, pp. 1413–1421.

[4] Y. Jia, M. Salzmann, and T. Darrell, "Factorized latent spaces with structured sparsity," in *Proc. Adv. Neural Inf. Process. Syst.*, 2010, pp. 982–990.

[5] Y. Han, F. Wu, D. Tao, J. Shao, Y. Zhuang, and J. Jiang, "Sparse unsupervised dimensionality reduction for multiple view data," *IEEE Trans. Circuits Syst. Video Technol.*, vol. 22, no. 10, pp. 1485–1496, Oct. 2012.

[6] J. Kim, R. D. C. Monteiro, and H. Park, "Group sparsity in nonnegative matrix factorization," in *Proc. SDM*, 2012, pp. 851–862.

[7] R. Jenatton, G. Obozinski, and F. Bach. (2009). "Structured sparse principal component analysis." [Online]. Available: http://arxiv.org/abs/0909.1440

[8] D. D. Lee and H. S. Seung, "Algorithms for non-negative matrix factorization," in *Proc. Adv. Neural Inf. Process. Syst.*, 2001, pp. 556–562.

[9] M. Wang, X.-S. Hua, R. Hong, J. Tang, G.-J. Qi, and Y. Song, "Unified video annotation via multigraph learning," *IEEE Trans. Circuits Syst. Video Technol.*, vol. 19, no. 5, pp. 733–746, May 2009.

[10] H. Wang, F. Nie, H. Huang, and C. Ding, "Heterogeneous visual features fusion via sparse multimodal machine," in *Proc. IEEE Conf. Comput. Vis. Pattern Recognit. (CVPR)*, Jun. 2013, pp. 3097–3102.

[11] Y. Han, Y. Yang, F. Wu, and R. Hong, "Compact and discriminative descriptor inference using multi-cues," *IEEE Trans. Image Process.*, vol. 24, no. 12, pp. 5114–5126, Dec. 2015.

[12] Z. Xue, G. Li, and Q. Huang, "Joint multi-view representation learning and image tagging," in *Proc. 30th AAAI Conf. Artif. Intell.*, 2016, pp. 1366–1372.

[13] H. Wang, F. Nie, and H. Huang, "Multi-view clustering and feature learning via structured sparsity," in *Proc. 30th Int. Conf. Mach. Learn. (ICML)*, 2013, pp. 352–360.

[14] Z. Xue, G. Li, S. Wang, C. Zhang, W. Zhang, and Q. Huang, "GOMES: A group-aware multi-view fusion approach towards real-world image clustering," in *Proc. IEEE Int. Conf. Multimedia Expo (ICME)*, Jun./Jul. 2015, pp. 1–6.

[15] L. Chu, Y. Zhang, G. Li, S. Wang, W. Zhang, and Q. Huang, "Effective multimodality fusion framework for cross-media topic detection," *IEEE Trans. Circuits Syst. Video Technol.*, vol. 26, no. 3, pp. 556–569, Mar. 2016.

[16] C. Xu, D. Tao, and C. Xu. (2013). "A survey on multi-view learning." [Online]. Available: https://arxiv.org/abs/1304.5634

[17] K. Chaudhuri, S. M. Kakade, K. Livescu, and K. Sridharan, "Multi-view clustering via canonical correlation analysis," in *Proc. 26th Annu. Int. Conf. Mach. Learn.*, 2009, pp. 129–136.

[18] X. Cai, F. Nie, H. Huang, and F. Kamangar, "Heterogeneous image feature integration via multi-modal spectral clustering," in *Proc. IEEE Conf. Comput. Vis. Pattern Recognit. (CVPR)*, Jun. 2011, pp. 1977–1984.

[19] H.-C. Huang, Y.-Y. Chuang, and C.-S. Chen, "Affinity aggregation for spectral clustering," in *Proc. IEEE Conf. Comput. Vis. Pattern Recognit. (CVPR)*, Jun. 2012, pp. 773–780.

[20] X. Cai, F. Nie, W. Cai, and H. Huang, "Heterogeneous image features integration via multi-modal semi-supervised learning model," in *Proc. IEEE Int. Conf. Comput. Vis. (ICCV)*, Dec. 2013, pp. 1737–1744.

[21] J. Gui, D. Tao, Z. Sun, Y. Luo, X. You, and Y. Y. Tang, "Group sparse multiview patch alignment framework with view consistency for image classification," *IEEE Trans. Image Process.*, vol. 23, no. 7, pp. 3126–3137, Jul. 2014.

[22] A. Blum and T. Mitchell, "Combining labeled and unlabeled data with co-training," in *Proc. 11th Annu. Conf. Comput. Learn. Theory*, 1998, pp. 92–100.

[23] A. Kumar and H. Daumé, "A co-training approach for multi-view spectral clustering," in *Proc. 28th Int. Conf. Mach. Learn. (ICML)*, 2011, pp. 393–400.

[24] Y.-Y. Lin, T.-L. Liu, and C.-S. Fuh, "Multiple kernel learning for dimensionality reduction," *IEEE Trans. Pattern Anal. Mach. Intell.*, vol. 33, no. 6, pp. 1147–1160, Jun. 2011.

[25] J. Liu, Y. Jiang, Z. Li, Z.-H. Zhou, and H. Lu, "Partially shared latent factor learning with multiview data," *IEEE Trans. Neural Netw. Learn. Syst.*, vol. 26, no. 6, pp. 1233–1246, Jun. 2014.

[26] C. Zhang, C. Liang, L. Li, J. Liu, Q. Huang, and Q. Tian, "Fine-grained image classification via low-rank sparse coding with general and class-specific codebooks," *IEEE Trans. Neural Netw. Learn. Syst.* [Online]. Available: http://ieeexplore.ieee.org/document/7448920/

[27] H. S. Seung and D. D. Lee, "The manifold ways of perception," *Science*, vol. 290, no. 5500, pp. 2268–2269, 2000.

[28] J. B. Tenenbaum, V. de Silva, and J. C. Langford, "A global geometric framework for nonlinear dimensionality reduction," *Science*, vol. 290, no. 5500, pp. 2319–2323, Dec. 2000.

[29] X. He and P. Niyogi, "Locality preserving projections," in *Advances in Neural Information Processing Systems*, vol. 16. Cambridge, MA, USA: MIT Press, 2004, p. 153.

[30] S. T. Roweis and L. K. Saul, "Nonlinear dimensionality reduction by locally linear embedding," *Science*, vol. 290, no. 5500, pp. 2323–2326, Dec. 2000.

[31] F. Nie, D. Xu, I. W. Tsang, and C. Zhang, "Flexible manifold embedding: A framework for semi-supervised and unsupervised dimension reduction," *IEEE Trans. Image Process.*, vol. 19, no. 7, pp. 1921–1932, Jul. 2010.

[32] F. Nie, S. Xiang, Y. Song, and C. Zhang, "Orthogonal locality minimizing globality maximizing projections for feature extraction," *Opt. Eng.*, vol. 48, no. 1, p. 017202, 2009.

[33] Y. Liu, B. Liao, and Y. Han, "Discriminative multi-view feature selection and fusion," in *Proc. IEEE Int. Conf. Multimedia Expo (ICME)*, Jun./Jul. 2015, pp. 1–6.

[34] C. Zhang, Q. Huang, and Q. Tian, "Contextual exemplar classifier based image representation for classification," *IEEE Trans. Circuits Syst. Video Technol.* [Online]. Available: http://ieeexplore.ieee.org/document/7401002/

[35] M. Belkin and P. Niyogi, "Laplacian eigenmaps and spectral techniques for embedding and clustering," in *Proc. NIPS*, vol. 14. 2001, pp. 585–591.

[36] F. Nie, C. Ding, D. Luo, and H. Huang, "Improved minmax cut graph clustering with nonnegative relaxation," in *Proc. Eur. Conf. Mach. Learn. Knowl. Discovery Databases*, 2010, pp. 451–466.

[37] L. Chu, S. Wang, S. Liu, Q. Huang, and J. Pei, "ALID: Scalable dominant cluster detection," *Proc. VLDB Endowment*, vol. 8, no. 8, pp. 826–837, 2015.

[38] D. Cai, X. He, J. Han, and T. S. Huang, "Graph regularized nonnegative matrix factorization for data representation," *IEEE Trans. Pattern Anal. Mach. Intell.*, vol. 33, no. 8, pp. 1548–1560, Aug. 2011.

[39] Z. Zhang and K. Zhao, "Low-rank matrix approximation with manifold regularization," *IEEE Trans. Pattern Anal. Mach. Intell.*, vol. 35, no. 7, pp. 1717–1729, Jul. 2013.

[40] L. Zhang, Q. Zhang, L. Zhang, D. Tao, X. Huang, and B. Du, "Ensemble manifold regularized sparse low-rank approximation for multiview feature embedding," *Pattern Recognit.*, vol. 48, no. 10, pp. 3102–3112, 2015.

[41] Q. Gu, C. Ding, and J. Han, "On trivial solution and scale transfer problems in graph regularized NMF," in *Proc. Int. Joint Conf. Artif. Intell. (IJCAI)*, 2011, vol. 22. no. 1, p. 1288.

[42] M. Sun and H. Van Hamme, "Large scale graph regularized non-negative matrix factorization with ℓ_1 normalization based on Kullback–Leibler divergence," *IEEE Trans. Signal Process.*, vol. 60, no. 7, pp. 3876–3880, Jul. 2012.

[43] L. Du and Y.-D. Shen, "Towards robust co-clustering," in *Proc. Int. Joint Conf. Artif. Intell. (IJCAI)*, 2013, pp. 1317–1322.

[44] J. Huang, F. Nie, H. Huang, and C. Ding, "Robust manifold nonnegative matrix factorization," *ACM Trans. Knowl. Discovery Data*, vol. 8, no. 3, 2014, Art. no. 11.

[45] F. Nie, H. Huang, X. Cai, and C. H. Ding, "Efficient and robust feature selection via joint $\ell_{2,1}$-norms minimization," in *Proc. Adv. Neural Inf. Process. Syst.*, 2010, pp. 1813–1821.

[46] D. Kong, C. Ding, and H. Huang, "Robust nonnegative matrix factorization using L21-norm," in *Proc. 20th ACM Int. Conf. Inf. Knowl. Manage.*, 2011, pp. 673–682.

[47] Y. Yang, H. T. Shen, Z. Ma, Z. Huang, and X. Zhou, "$\ell_{2,1}$-norm regularized discriminative feature selection for unsupervised learning," in *Proc. Int. Joint Conf. Artif. Intell. (IJCAI)*, 2011, vol. 22. no. 1, p. 1589.

[48] F. Nie, J. Yuan, and H. Huang, "Optimal mean robust principal component analysis," in *Proc. 31st Int. Conf. Mach. Learn. (ICML)*, 2014, pp. 1062–1070.

[49] X. He, M.-Y. Kan, P. Xie, and X. Chen, "Comment-based multi-view clustering of Web 2.0 items," in *Proc. 23rd Int. Conf. World Wide Web*, 2014, pp. 771–782.

[50] Q. Gu and J. Zhou, "Co-clustering on manifolds," in *Proc. 15th ACM SIGKDD Int. Conf. Knowl. Discovery Data Mining*, 2009, pp. 359–368.

[51] T.-S. Chua, J. Tang, R. Hong, H. Li, Z. Luo, and Y. Zheng, "NUS-WIDE: A real-world Web image database from National University of Singapore," in *Proc. ACM Int. Conf. Image Video Retr.*, 2009, Art. no. 48.

[52] M. Everingham, L. van Gool, C. Williams, J. Winn, and A. Zisserman. *The PASCAL Visual Object Classes Challenge 2007 (VOC2007) Results*.

[53] M. A. Stricker and M. Orengo, "Similarity of color images," *Proc. SPIE*, vol. 2420, pp. 381–392, Mar. 1995.

[54] D. G. Lowe, "Distinctive image features from scale-invariant keypoints," *Int. J. Comput. Vis.*, vol. 60, no. 2, pp. 91–110, 2004.

[55] N. Dalal and B. Triggs, "Histograms of oriented gradients for human detection," in *Proc. IEEE Comput. Soc. Conf. Comput. Vis. Pattern Recognit. (CVPR)*, vol. 1. Jun. 2005, pp. 886–893.

[56] A. Oliva and A. Torralba, "Modeling the shape of the scene: A holistic representation of the spatial envelope," *Int. J. Comput. Vis.*, vol. 42, no. 3, pp. 145–175, 2001.

[57] T. Ojala, M. Pietikäinen, and T. Mäenpää, "Multiresolution gray-scale and rotation invariant texture classification with local binary patterns," *IEEE Trans. Pattern Anal. Mach. Intell.*, vol. 24, no. 7, pp. 971–987, Jul. 2002.

[58] H. Wang, C. Weng, and J. Yuan, "Multi-feature spectral clustering with minimax optimization," in *Proc. IEEE Conf. Comput. Vis. Pattern Recognit. (CVPR)*, Jun. 2014, pp. 4106–4113.

[59] T. Fawcett, "An introduction to ROC analysis," *Pattern Recognit. Lett.*, vol. 27, no. 8, pp. 861–874, Jun. 2006.

Zhe Xue received the B.S. degree in electronic engineering from Civil Aviation University of China, Tianjin, China, in 2010. He is currently working toward the Ph.D. degree with University of Chinese Academy of Sciences, Beijing, China.

His research interests include machine learning, pattern recognition, computer vision, and multimedia data mining.

Guorong Li received the B.S. degree in computer science from Renmin University of China, Beijing, China, in 2006 and the Ph.D. degree in computer science from University of Chinese Academy of Sciences, Beijing, in 2012.

She is an Associate Professor with University of Chinese Academy of Sciences. Her research interests include object tracking, pattern recognition, cross-media analysis, and multilabel learning.

Shuhui Wang received the B.S. degree in electronic engineering from Tsinghua University, Beijing, China, in 2006 and the Ph.D. degree from the Institute of Computing Technology, Chinese Academy of Sciences, Beijing, in 2012.

He is a Researcher with the Key Laboratory of Intelligent Information Processing of Chinese Academy of Sciences, Institute of Computing Technology, Chinese Academy of Sciences. His research interests include semantic image analysis, image and video retrieval, and large-scale web multimedia data mining.

Weigang Zhang received the B.S., M.S., and Ph.D. degrees in computer science from the Harbin Institute of Technology (HIT), Harbin, China, in 2003, 2005, and 2016, respectively.

He is an Associate Professor with the School of Computer Science and Technology, HIT, Weihai, China, and is also a Post-Doctoral Researcher with the University of Chinese Academy of Sciences, CAS, Beijing, China. His current research interests include multimedia analysis, video processing, and cross-media computing.

Qingming Huang (SM'08) is currently a Professor and a Deputy Dean with the School of Computer and Control Engineering, University of Chinese Academy of Sciences, Beijing, China. He has published over 300 academic papers in international journals, such as the IEEE TRANSACTIONS ON IMAGE PROCESSING, the IEEE TRANSACTIONS ON MULTIMEDIA, the IEEE TRANSACTIONS ON CIRCUITS AND SYSTEMS FOR VIDEO TECHNOLOGY, and top level international conferences, including ACM Multimedia, ICCV, CVPR, VLDB, IJCAI. His current research interests include multimedia computing, image/video processing, pattern recognition, and computer vision.